REPORT DOCUMENTATION PAGE

1. REPORT DATE *(DD-MM-YYYY)*	2. REPORT TYPE		3. DATES COVERED *(From - To)*
	Technical Papers		

4. TITLE AND SUBTITLE	5a. CONTRACT NUMBER
	5b. GRANT NUMBER
	5c. PROGRAM ELEMENT NUMBER

6. AUTHOR(S)	5d. PROJECT NUMBER
	2303
	5e. TASK NUMBER
	M2C8
	5f. WORK UNIT NUMBER

7. PERFORMING ORGANIZATION NAME(S) AND ADDRESS(ES)	8. PERFORMING ORGANIZATION REPORT
Air Force Research Laboratory (AFMC) AFRL/PRS 5 Pollux Drive Edwards AFB CA 93524-7048	

9. SPONSORING / MONITORING AGENCY NAME(S) AND ADDRESS(ES)	10. SPONSOR/MONITOR'S ACRONYM(S)
Air Force Research Laboratory (AFMC) AFRL/PRS 5 Pollux Drive Edwards AFB CA 93524-7048	11. SPONSOR/MONITOR'S NUMBER(S)

12. DISTRIBUTION / AVAILABILITY STATEMENT

Approved for public release; distribution unlimited.

13. SUPPLEMENTARY NOTES

14. ABSTRACT

1121   036

15. SUBJECT TERMS

16. SECURITY CLASSIFICATION OF:			17. LIMITATION OF ABSTRACT	18. NUMBER OF PAGES	19a. NAME OF RESPONSIBLE PERSON Leilani Richardson
a. REPORT	b. ABSTRACT	c. THIS PAGE	A		19b. TELEPHONE NUMBER *(include area code)* (661) 275-5015
Unclassified	Unclassified	Unclassified			

MEMORANDUM FOR PRR (In-House Publication)

24 May 1999

FROM: PROI (TI) (STINFO)

SUBJECT: Authorization for Release of Technical Information, Control Number: AFRL-PR-ED-TP-FY99-0107
Bill Larson, "Identification and Condensation of Cyclic C_6 and Cyclic C_8 in Solid Argon and Matrix-Isolated
Boron/Carbon"

Presentation

(Public Release)

Identification and condensation of cyclic C_6 and cyclic C_8 in solid argon

Characterization of matrix isolated $B_J C_{n-J}$ J=0, 1, 2;   n=3-11 in solid argon

C. William Larson
Propulsion Directorate
Air Force Research Laboratory
Edwards AFB, CA 93524-7680

HEDM RESEARCH GROUP
Pat Carrick (Chief), Jeff Sheehy (Group Leader), Greg Drake, Hi Young Yoo, Jeffrey Mills, Jerry Boatz, Jessica Harper, Karl Christe, Mario Fajardo, Michael Tinnirello, Michelle DeRose, Paul Jones, Txomin Presilla (Schafer Corporation) Peter Langhoff, Simon Tam, Suresh Suri, William Wilson

University of Florida
Department of Chemistry
Gainesville, Florida
June 8, 1999

20021121 036

Rocket Science

$$\frac{m_{final}}{m_{initial}} = \exp -\frac{\Delta V}{g I_{sp}}$$

$$I_{sp} = \frac{1}{g}\sqrt{2(h_{propellant} - h_{exit})}$$

$h = enthalpy\ per\ unit\ mass$

SSME

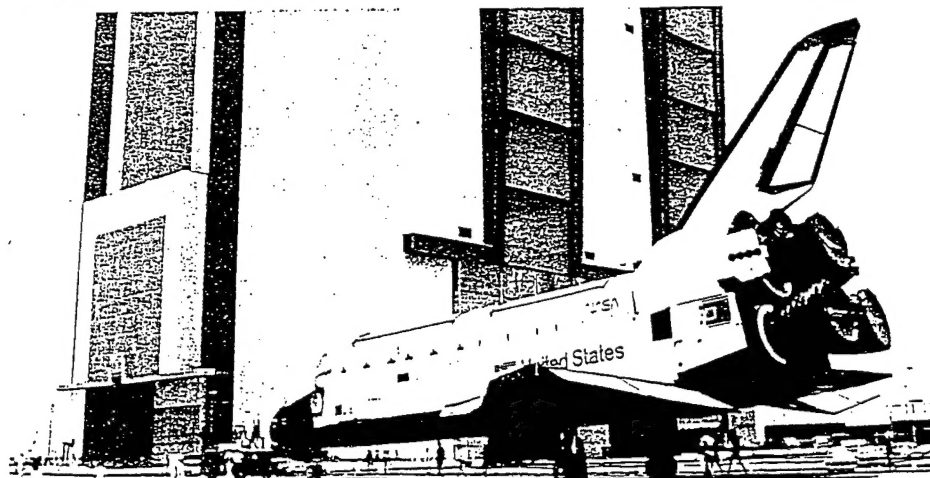**Rockwell International**
Rocketdyne Division

SPACE SHUTTLE MAIN ENGINE

The Space Shuttle Main Engine (SSME) was developed expressly for use on America's Space Shuttle. Using a mixture of liquid oxygen and liquid hydrogen, the SSME can attain a maximum thrust level (in vacuum) of 512,300 pounds at 109% power level. The regeneratively cooled engine also features high performance turbopumps for propellant and oxidizer that develop 77,310 horsepower and 29,430 horsepower, respectively. Ultra-high-pressure operation of the pumps and combustion chamber allows expansion of all hot gases through a high-area-ratio exhaust nozzle to achieve efficiencies never previously attained in a production rocket engine. These advantages allow a heavier payload to be carried without increasing launch vehicle size.

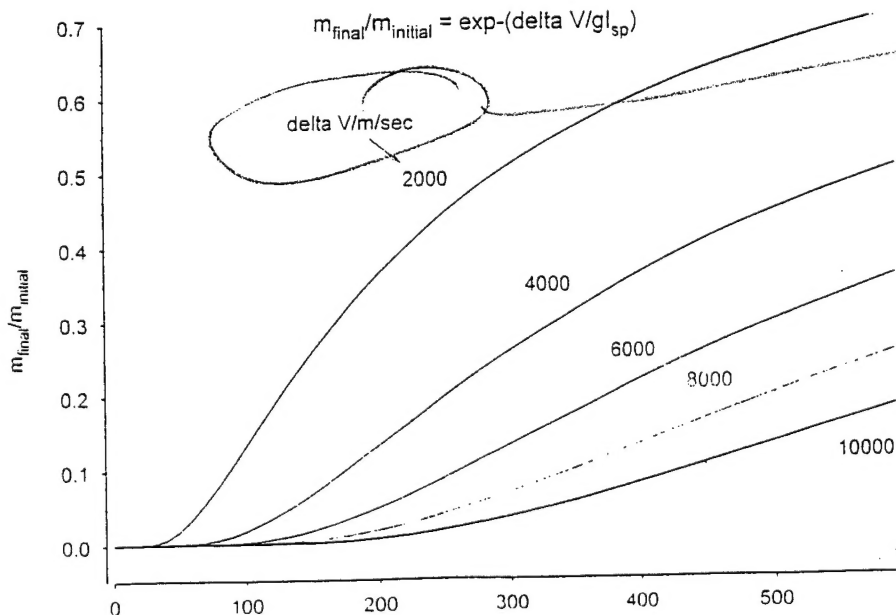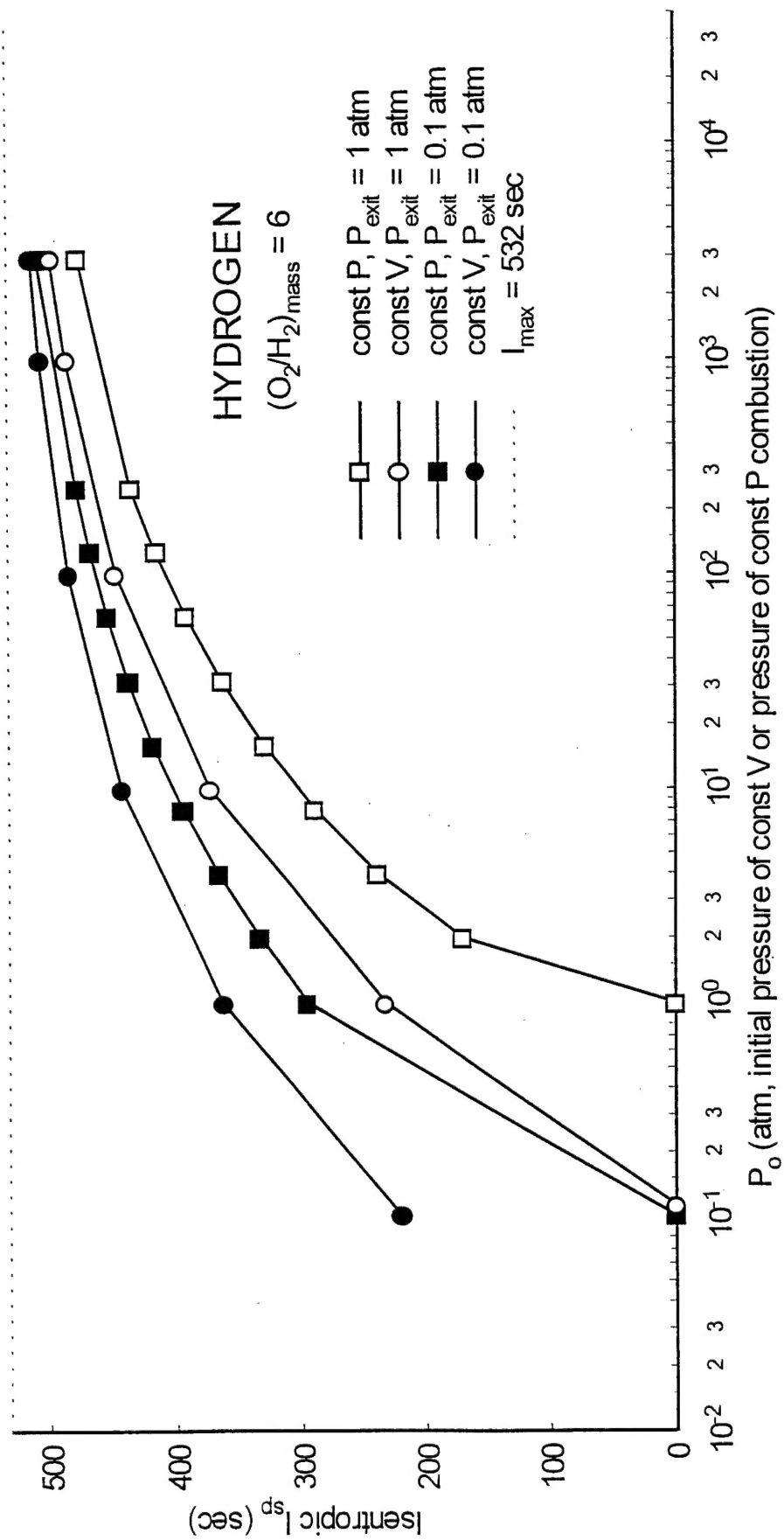### SPACE SHUTTLE MAIN ENGINE
PERFORMANCE (FULL POWER LEVEL)

Maximum Thrust: (109% Power Level)
At Sea Level .... 408,750 pounds
In Vacuum .... 2,290 kNt .... 512,300 pounds
Throttle Range .... 65% ~ 109%
Pressures:
Hydrogen Pump Discharge .... 7,040 psia
Oxygen Pump Discharge .... 8,070 psia
Chamber Pressure .... 3,260 psia
Specific Impulse (In Vacuum) ...... 4,444 m/s .... 453.5 seconds
Power: 5.07 GW (Exhaust, in vacuum)
High Pressure Pumps
Hydrogen .... 77,310 horsepower
Oxygen .... 29,430 horsepower
Area Ratio 77.5:1
Weight: .... 6.367 x 10⁷ kg/w .... 6,990 pounds
Mixture Ratio (O/F) 6.0:1
Dimensions: .... 168 in. long/96 in. wide
Propellants:
Fuel .... Liquid Hydrogen
Oxidizer .... Liquid Oxygen

For more information contact: ELV Propulsion/Rockwell International/Rocketdyne Division/6633 Canoga Ave./
Canoga Park/CA/91303/(818)700-6027

$$m_{final}/m_{initial} = \exp(-\Delta V/gI_{sp})$$

delta V/m/sec

2000

4000

6000

8000

10000

HYDROGEN

$(O_2/H_2)_{mass} = 6$

□ — const P, P_{exit} = 1 atm
○ — const V, P_{exit} = 1 atm
■ — const P, P_{exit} = 0.1 atm
● — const V, P_{exit} = 0.1 atm
.... I_{max} = 532 sec

P_o (atm, initial pressure of const V or pressure of const P combustion)
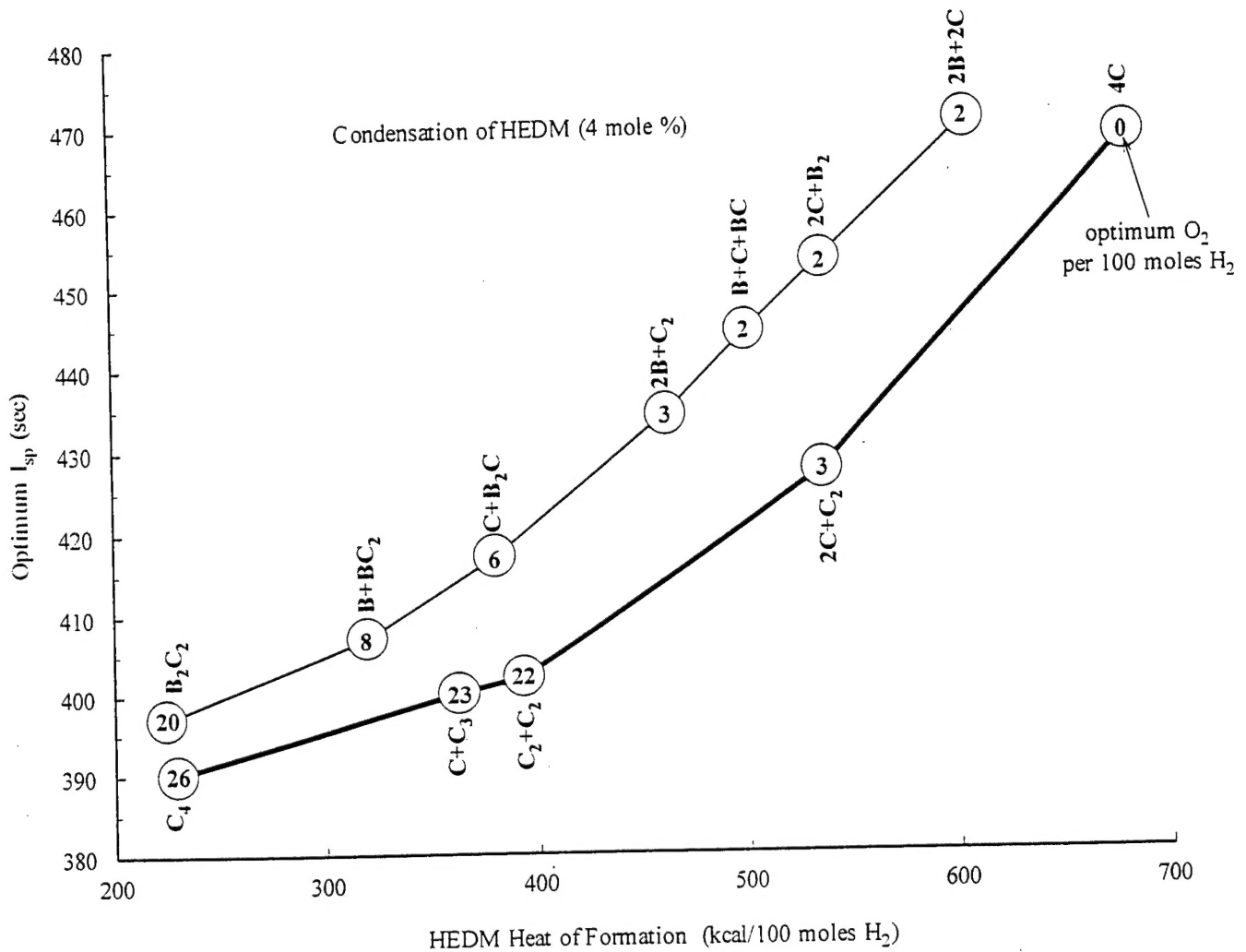
Isentropic I_{sp} (sec)

Figure 1. Specific impulse of HEDM containing 4 mole percent equivalent atom density in solid hydrogen with various stages of condensation. Numbers inside circles denote the optimum moles of O_2 per 100 moles of H_2 that produces the maximum Isp for the indicated compositions. The calculations are based on the standard rocket operating conditions, 1000 psi combustion pressure and 1 atm nozzle exit pressure, which produce 389 sec with liquid oxygen/liquid hydrogen propellant. The propellant composed of 4 mole percent C-atoms produces maximum Isp with no oxygen. If the atoms condense to 1 mole percent C4, the Isp drops to the baseline 389 sec value.
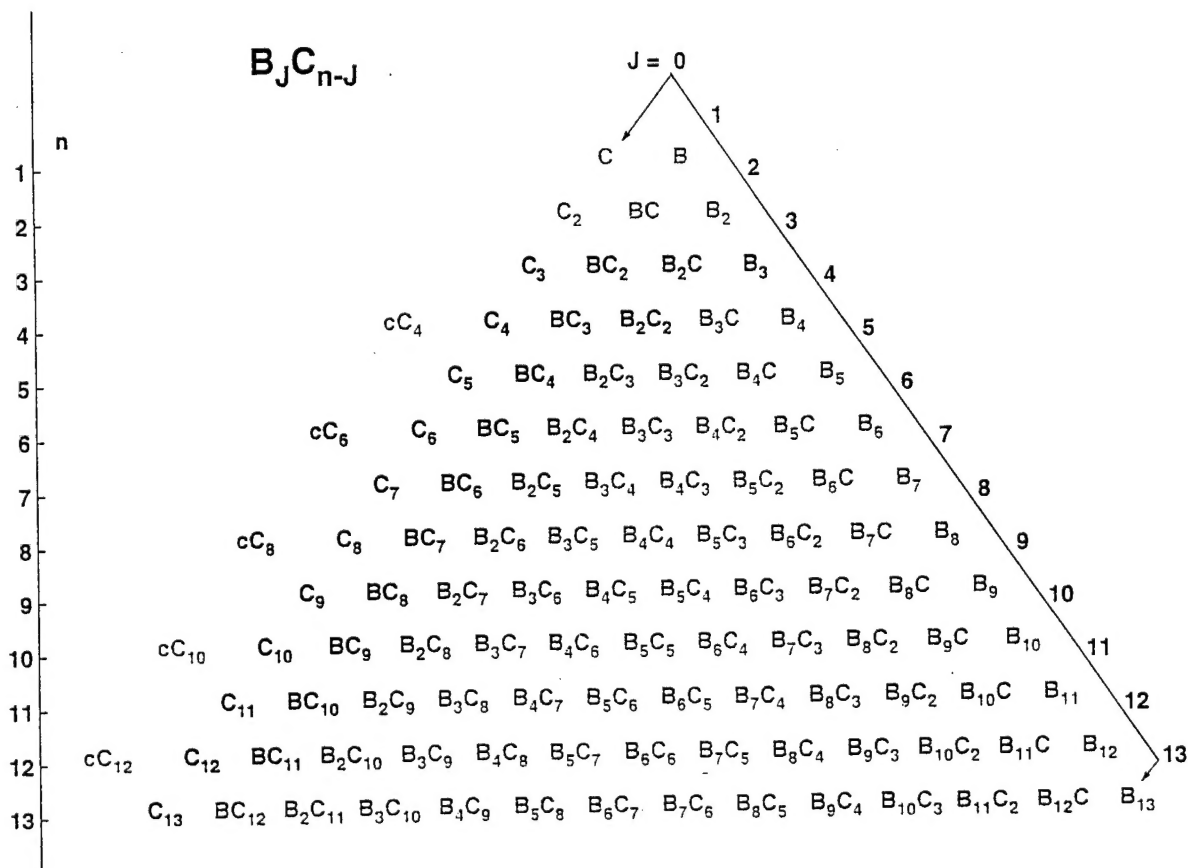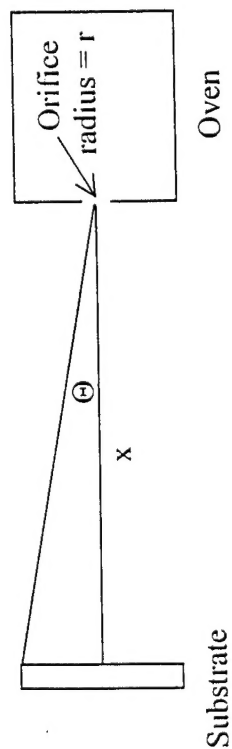
4

Objective - 5% atoms in cryogenic matrix

Approach

1. FTIR spectroscopy of $B_J C_{n-J}$ clusters isolated in 10 K argon matrix

2. Ab-initio calculations of cluster
   (a) normal mode frequencies and frequency shifts of their isotopomers
   (b) infrared absorption intensities (km mol^{-1})

3. Measurement of cluster distributions produced upon deposition and after annealing. Absolute column densities (molecules cm^{-2}) from Beer's Law

$$< \rho_i l > = \frac{A_{exp}}{I_{theory}} N$$

$$A_{exp} = - \int_\nu \ln \left[\frac{E_t(\nu)}{E_0(\nu)} \right] d\nu$$

$B_J C_{n-J}$

$J = 0$

	n													

C   B   1

2

1   C_2 BC B_2 3

2   C_3 BC_2 B_2C B_3 4

3   cC_4 C_4 BC_3 B_2C_2 B_3C B_4 5

4   C_5 BC_4 B_2C_3 B_3C_2 B_4C B_5 6

5   cC_6 C_6 BC_5 B_2C_4 B_3C_3 B_4C_2 B_5C B_6 7

6   C_7 BC_6 B_2C_5 B_3C_4 B_4C_3 B_5C_2 B_6C B_7 8

7   cC_8 C_8 BC_7 B_2C_6 B_3C_5 B_4C_4 B_5C_3 B_6C_2 B_7C B_8 9

8   C_9 BC_8 B_2C_7 B_3C_6 B_4C_5 B_5C_4 B_6C_3 B_7C_2 B_8C B_9 10

9   cC_{10} C_{10} BC_9 B_2C_8 B_3C_7 B_4C_6 B_5C_5 B_6C_4 B_7C_3 B_8C_2 B_9C B_{10} 11

10   C_{11} BC_{10} B_2C_9 B_3C_8 B_4C_7 B_5C_6 B_6C_5 B_7C_4 B_8C_3 B_9C_2 $B_{10}C$ B_{11} 12

11   cC_{12} C_{12} BC_{11} B_2C_{10} B_3C_9 B_4C_8 B_5C_7 B_6C_6 B_7C_5 B_8C_4 B_9C_3 $B_{10}C_2$ $B_{11}C$ B_{12} 13

12

13   C_{13} BC_{12} B_2C_{11} B_3C_{10} B_4C_9 B_5C_8 B_6C_7 B_7C_6 B_8C_5 B_9C_4 $B_{10}C_3$ $B_{11}C_2$ $B_{12}C$ B_{13}

Orifice
radius = r

Oven

Substrate

x

Θ
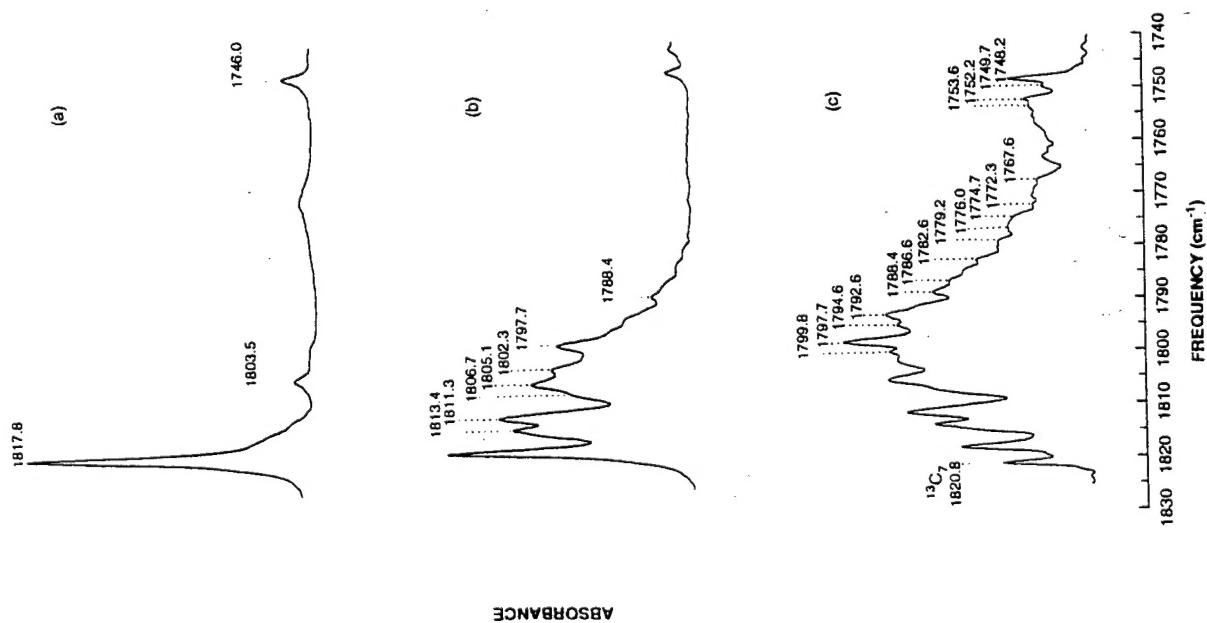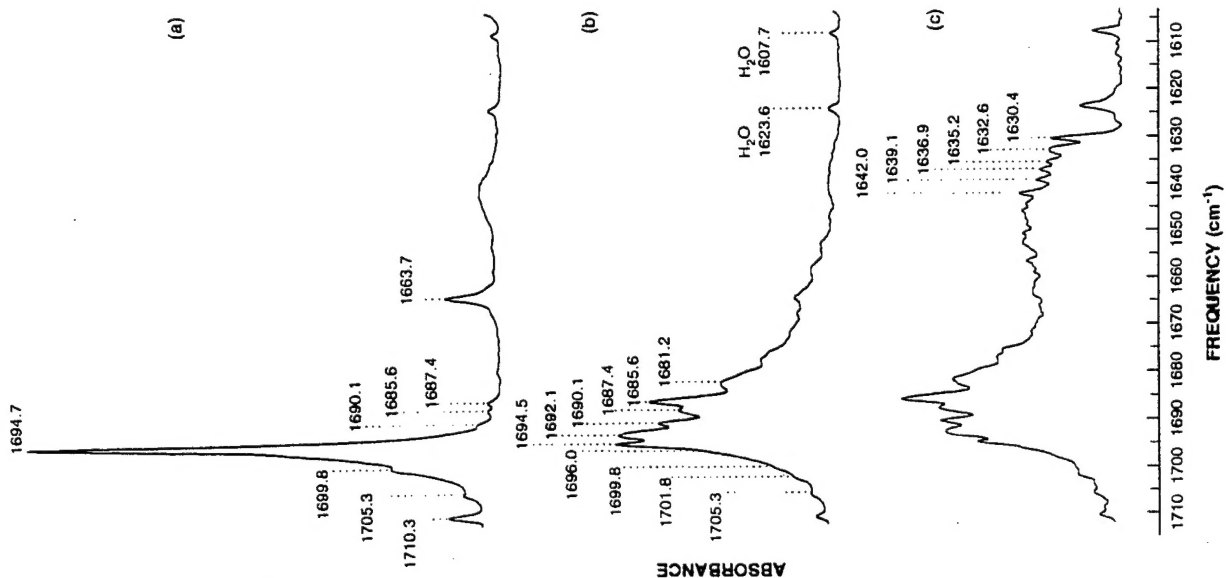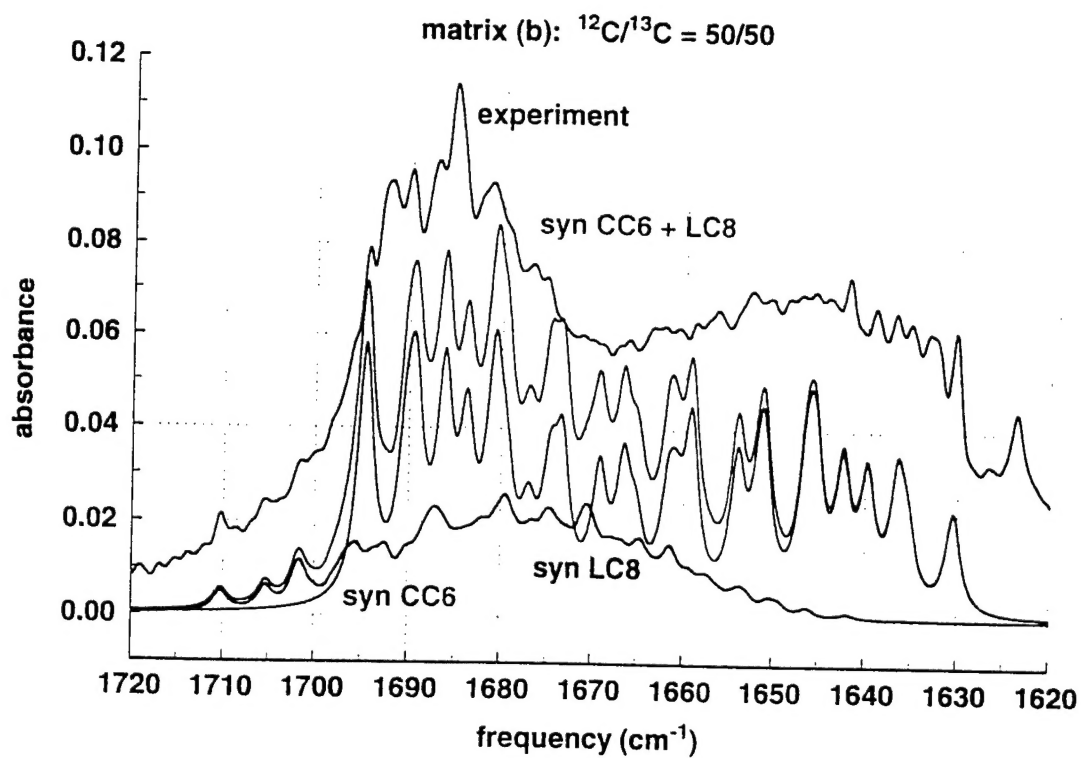
(1)　$Q_{atom}(\Theta, x) = \frac{1}{4}\rho \bar{c} a \dfrac{\cos^3\Theta}{\pi x^2}$

(2)　$Q_{rad}(\Theta, x) = \sigma T^4 a \dfrac{\cos^3\Theta}{\pi x^2}$

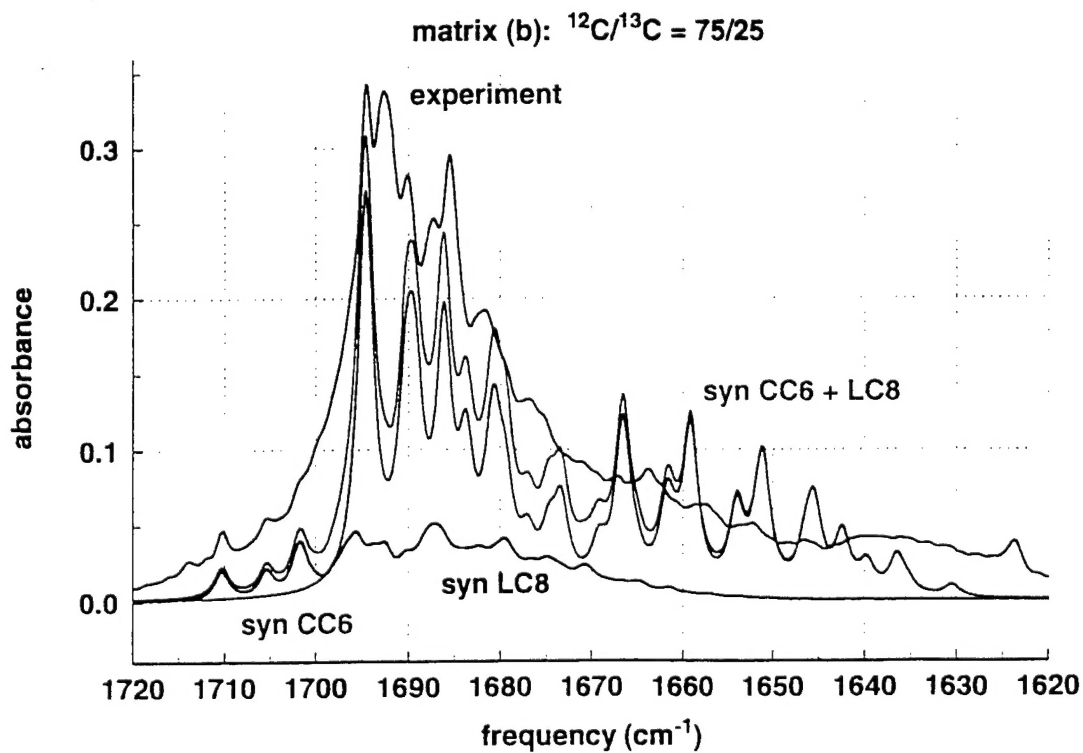Table I. Properties of a boron evaporation oven[a] , r = 0.05 cm, θ = 0

	x = 10 cm			x = 20 cm
P (Torr)	0.01	0.1	1	10
T (K)	2409	2631	2898	3230
ρ (#/cm^3)	4.01×10^{13}	3.67×10^{14}	3.33×10^{15}	2.98×10^{16}
$\bar{c}$ (cm/s)	2.13×10^5	2.24×10^5	2.35×10^5	2.48×10^5
Evap rate (#/s)	1.68×10^{16}	1.61×10^{17}	1.53×10^{18}	1.45×10^{19}
Evap rate (mg/hour)	1.11	10.6	101	957
λ (cm)[b]	100.0	10.9	1.20	0.134
Kn = $\lambda/2r$	1000	109	12.0	1.34
Q_{atom} (#/cm^2 s)	5.37×10^{13}	5.13×10^{14}	4.89×10^{15}	1.17×10^{16}
Q_{rad} (mW/cm^2)	4.74	6.75	9.93	3.78

(a) Based on vapor pressure data from Nesmeyanov's (1963) compilation, "Vapor Pressure of the Elements."
(b) Mean free path based on a collision diameter of 1.59×10^{-8} cm for boron + boron [Moelwyn-Hughes (1961), p25].
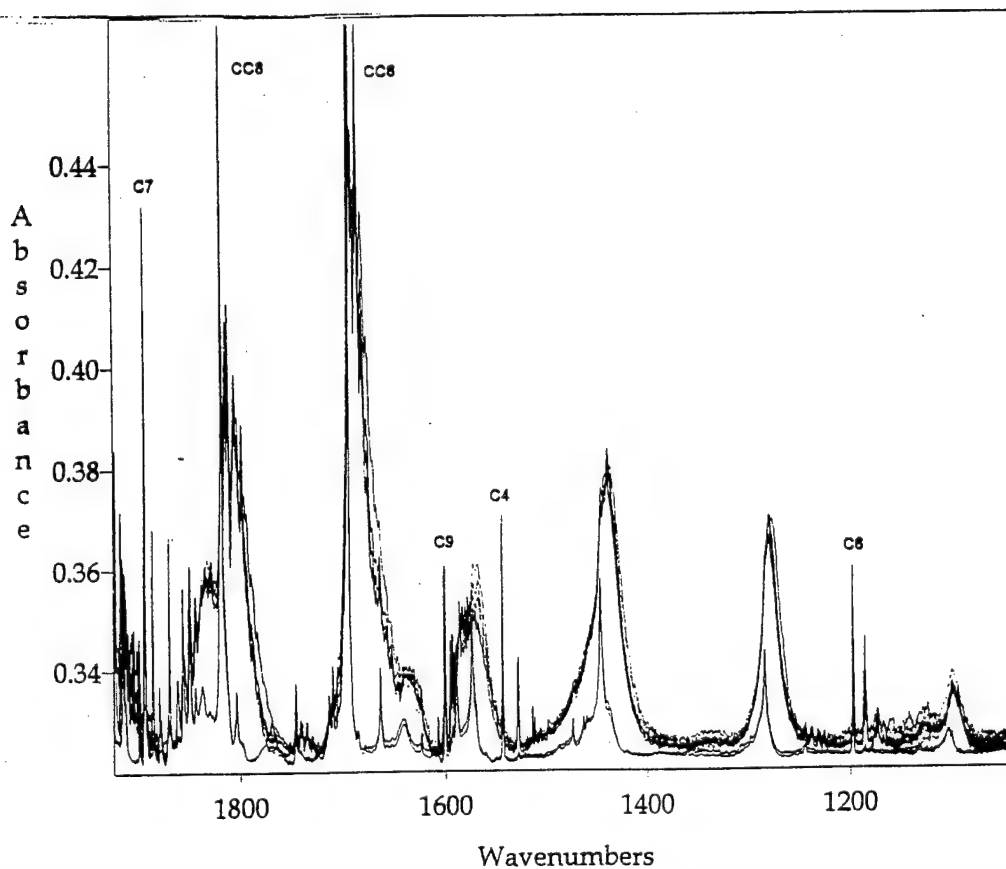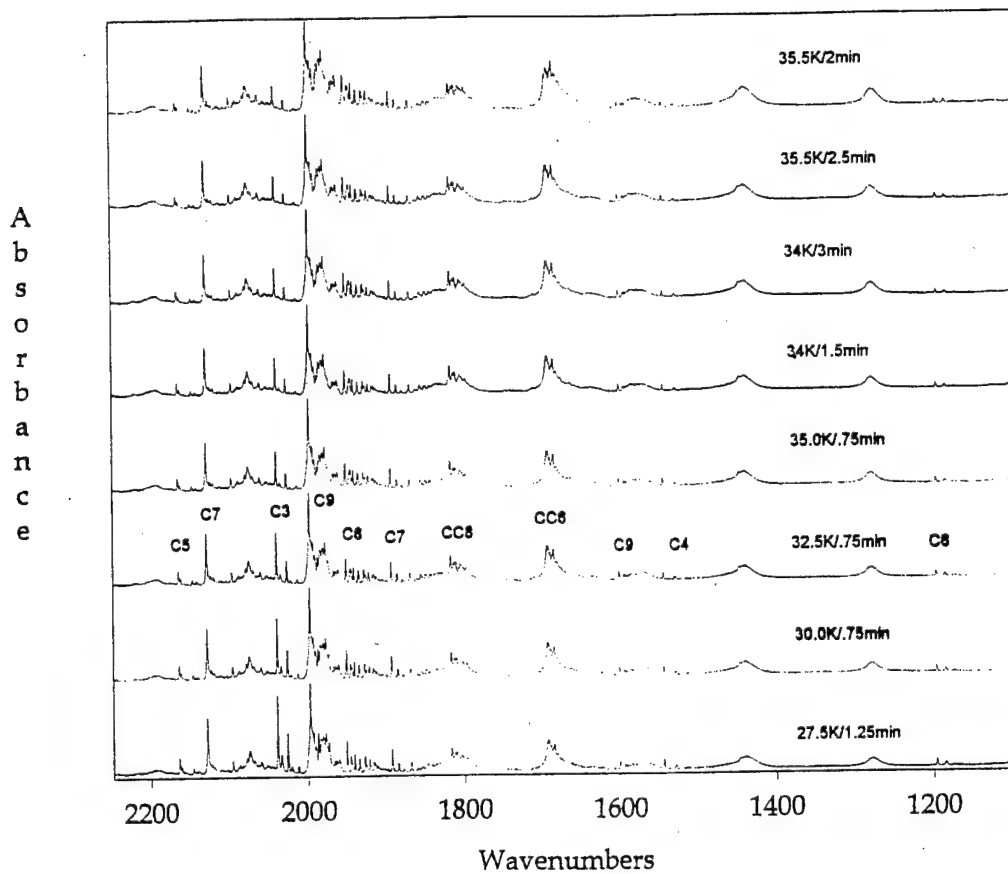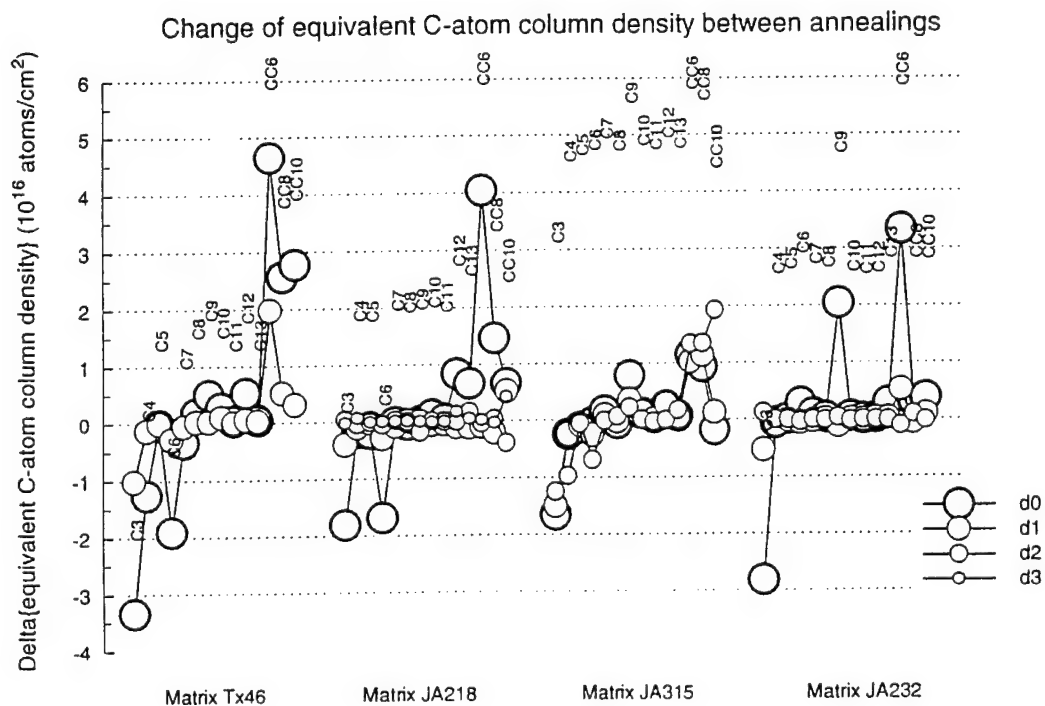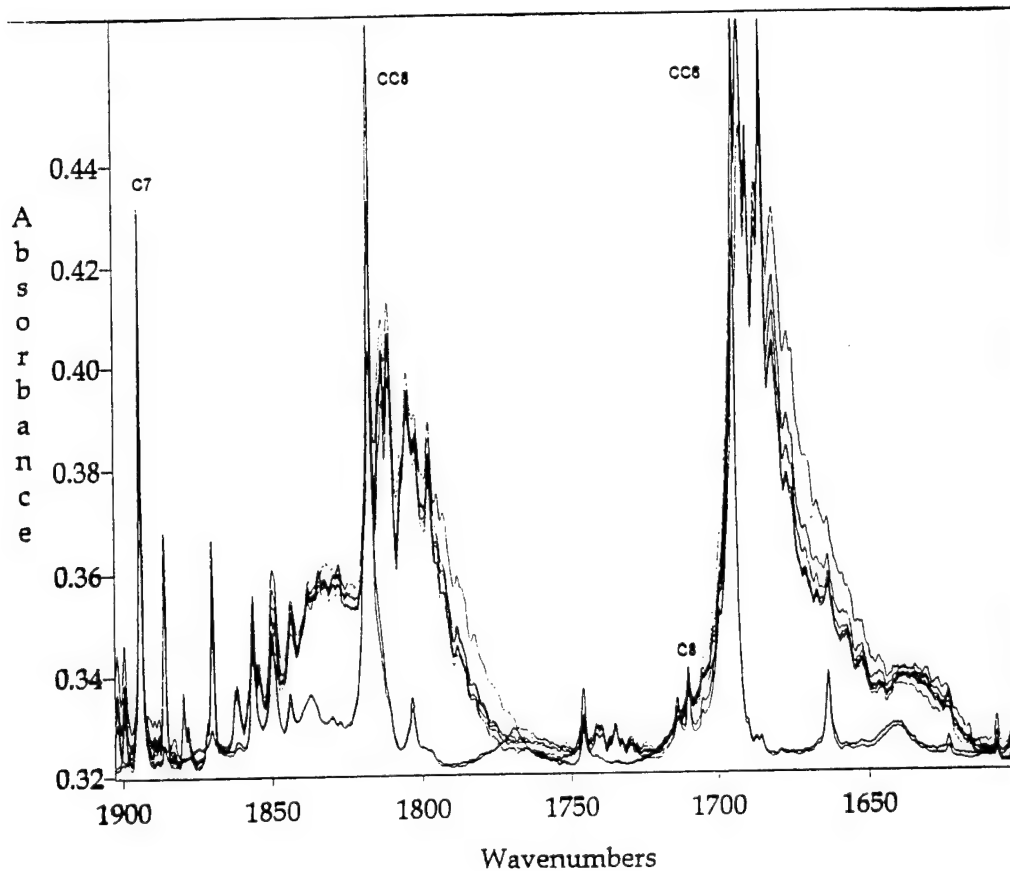
6

FREQUENCY (cm⁻¹)

ABSORBANCE

FREQUENCY (cm⁻¹)

ABSORBANCE

7

matrix (b): $^{12}C/^{13}C$ = 50/50

experiment

syn CC6 + LC8

syn LC8

syn CC6

absorbance

frequency (cm^{-1})

syncc67.axд

matrix (b): $^{12}C/^{13}C$ = 75/25

experiment

syn CC6 + LC8

syn LC8

syn CC6

absorbance

frequency (cm^{-1})

syncc68.axд

8

35.5K/2min

35.5K/2.5min

34K/3min

34K/1.5min

35.0K/.75min

C7   C3   C9
C5   C8   C7   CC8   CC6   C9   C4   32.5K/.75min   C6

30.0K/.75min

27.5K/1.25min

Wavenumbers

CC8   CC6

C7

C4

C9

C6

Wavenumbers

9

Top figure (Absorbance vs Wavenumbers)

A
b
s
o
r
b
a
n
c
e

0.44
0.42
0.40
0.38
0.36
0.34
0.32

1900 1850 1800 1750 1700 1650

Wavenumbers

C7 CC8 CC6 C8

Change of equivalent C-atom column density between annealings

Delta(equivalent C-atom column density) $(10^{16}\ atoms/cm^2)$

6
5
4
3
2
1
0
-1
-2
-3
-4

Matrix Tx46   Matrix JA218   Matrix JA315   Matrix JA232

CC6   CC6   CC6   CC6
CC8   CC8   CC8
CC10 CC10 CC10

C5 C7 C8 C9 C10 C11 C12 C13
C4 C5 C6 C3
C3 C6

C4 C5 C6 C7 C8 C9 C10 C11 C12 C13
C3 C5 C6 C8 C9 C10 C11 C12

d0
d1
d2
d3

Comparison of C_4/C_6, C_7/C_9, C_{10}/C_{12} Ratios
Obtained for Different Experimental Conditions
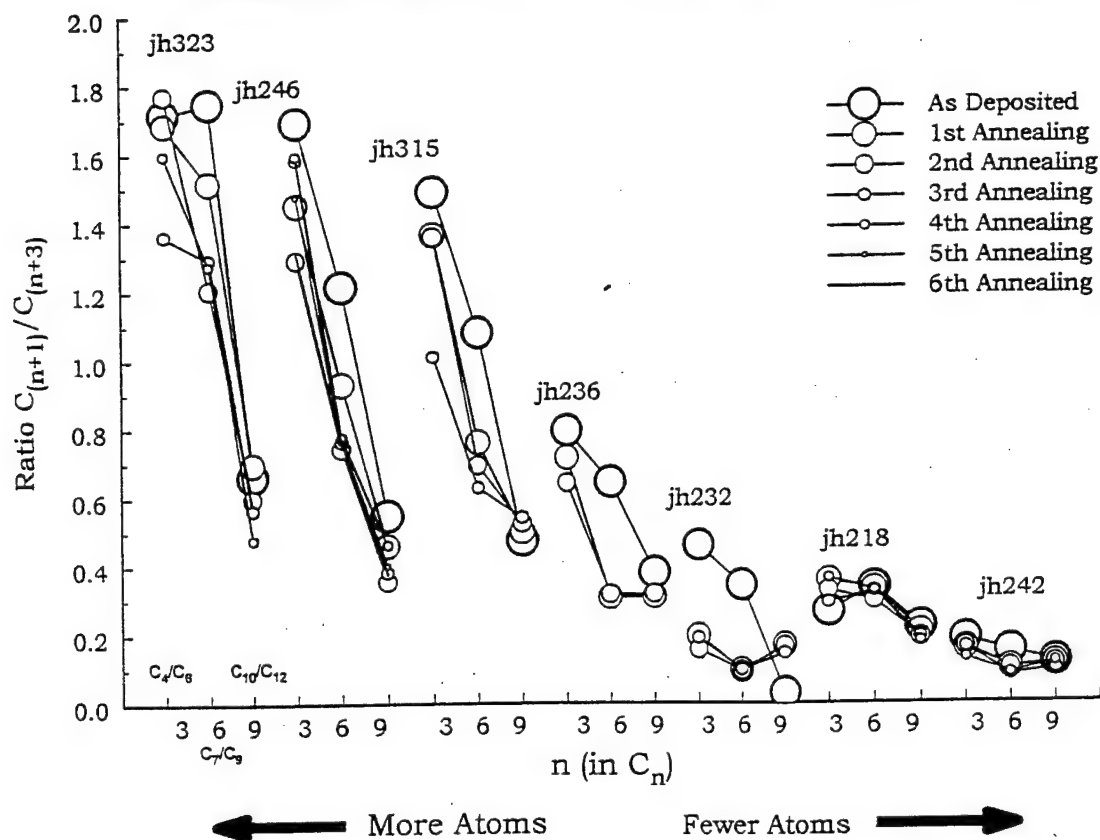
The ratio of the equivalent carbon atom column density for n+1 species (n as in C_n) to the equivalent carbon atom column density for n+3 species indicates how many atoms were available for formation of species like C_4, C_7, and C_{10}. When the Ta cell was hotter more n+1 species were formed during deposition than when the cell was colder. During annealings there were only minimal changes in the relative order of the ratios for C_4/C_6; C_7/C_9; C_{10}/C_{12}. Similar results are noted for $C(n+2)/C(n+3)$.

The run with 5% H_2/95% Ar yields a lower $C(n+1)/C(n+3)$ ratio than would be expected. The hydrogen may be scavenging atoms.

11

Comparison of C_5/C_6, C_8/C_9, C_{11}/C_{12} Ratios
Obtained for Different Experimental Conditions

Equivalent C-atom Column Density
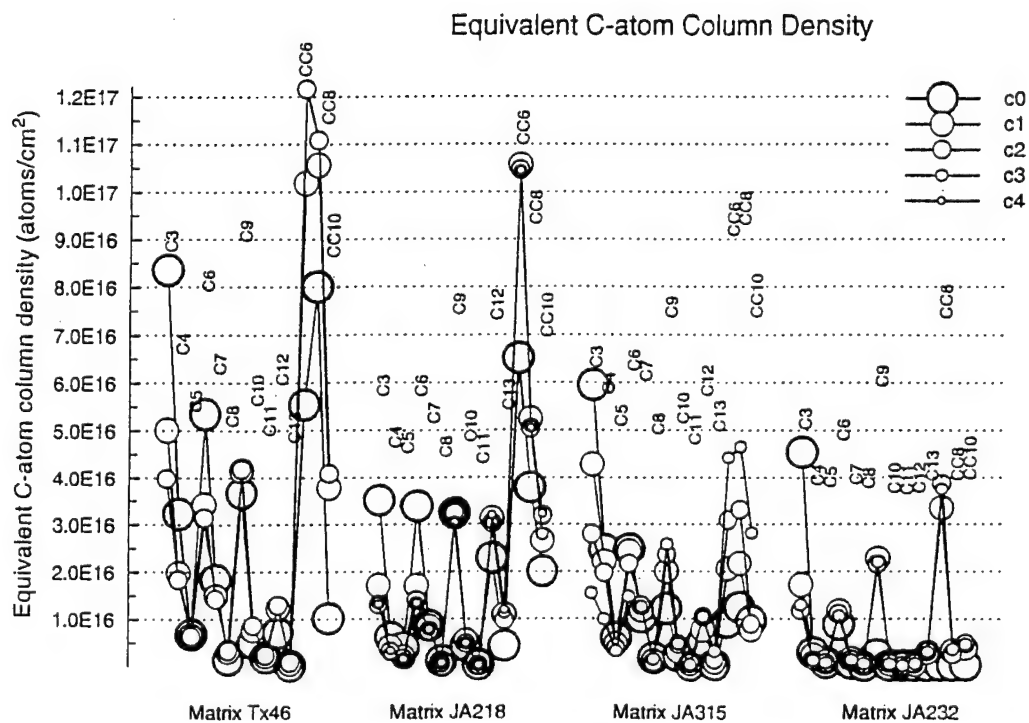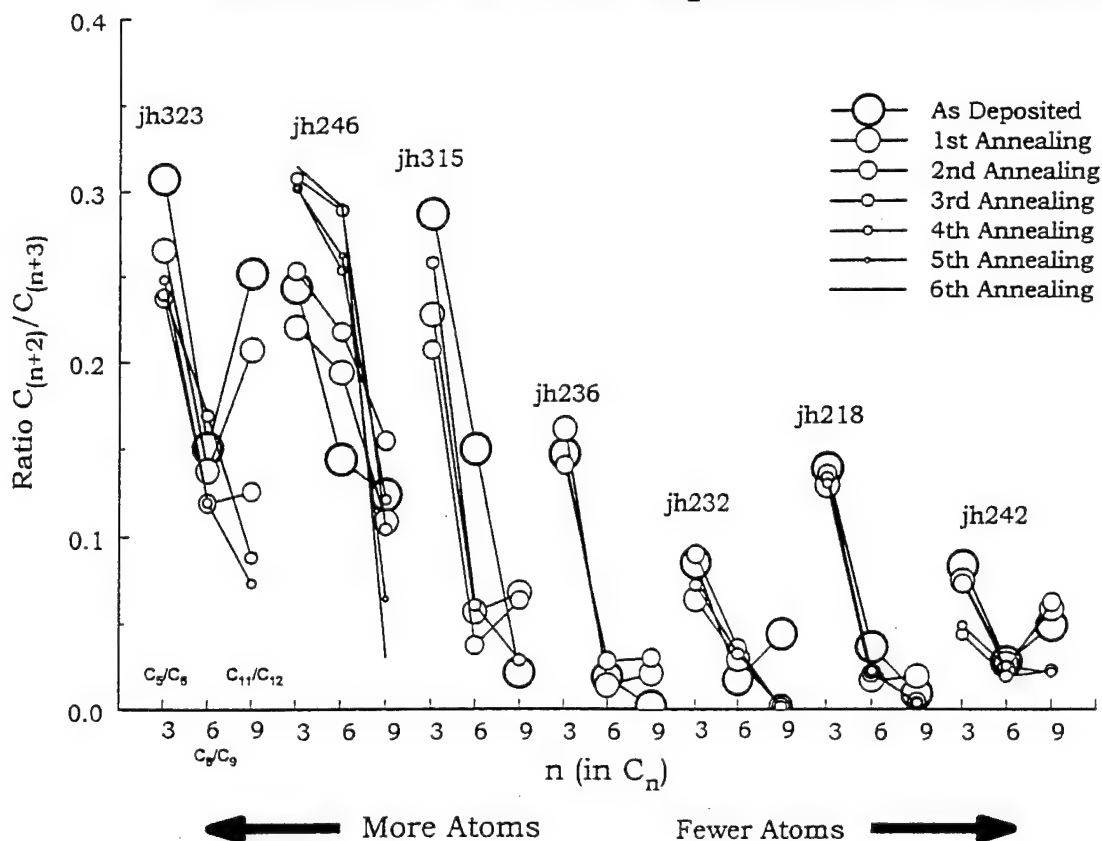
Cumulative Sum of Equivalent Carbon Atom Density
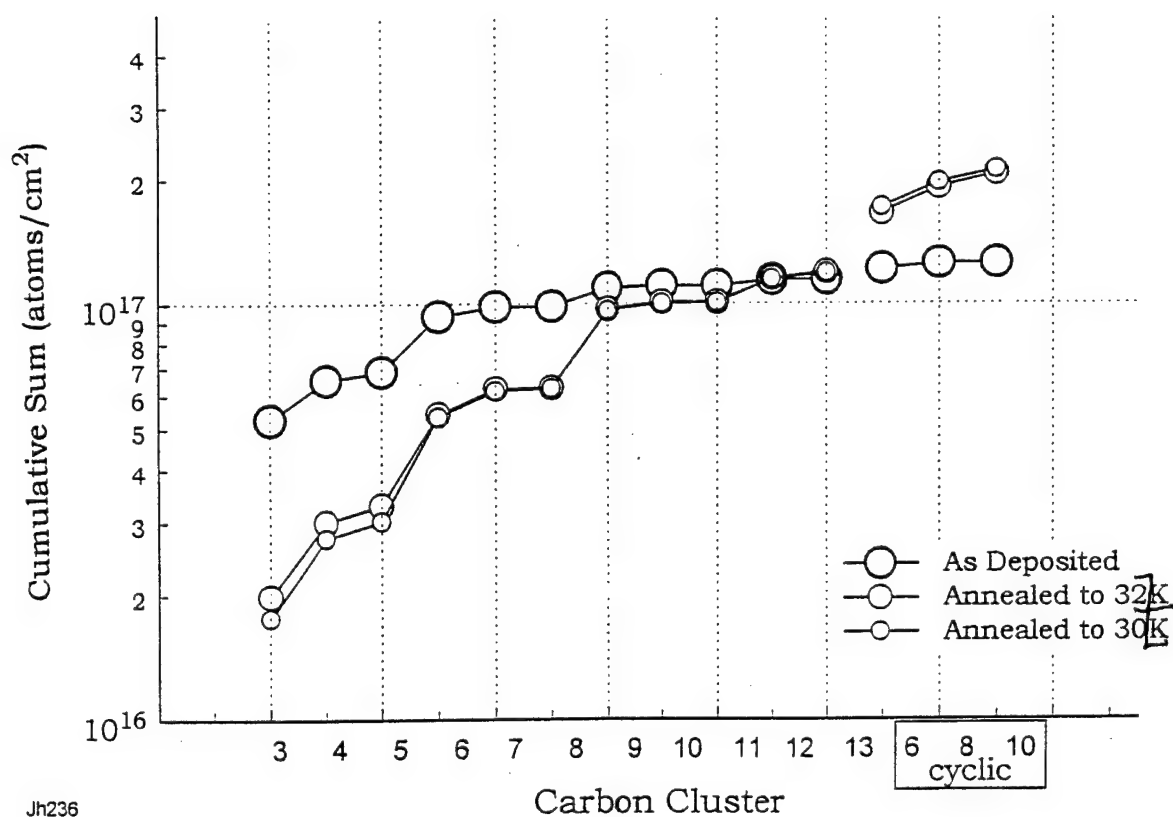
Jh236

From successive cluster distributions one can calculate the quantity of carbon species that were not detected in the as-deposited matrix IR spectrum. This increase in the total equivalent carbon atom density is attributed to carbon atoms that are "invisible" to IR and were thus not accounted for in the original IR spectrum.

13

1= MixG+L (2053.7,.0078452,1.7666,.44691)   2= MixG+L (2051.9,.027381,1.4388,1.00E-06)   3= MixG+L (2050.3,.064283,1.434,.10607)
4= MixG+L (2048.9,.0052507,1.2237,.99803)   5= MixG+L (2047.9,.014253,1.9605,.99103)   6= Quadr (-.41118,.000086926,2.15E-09)
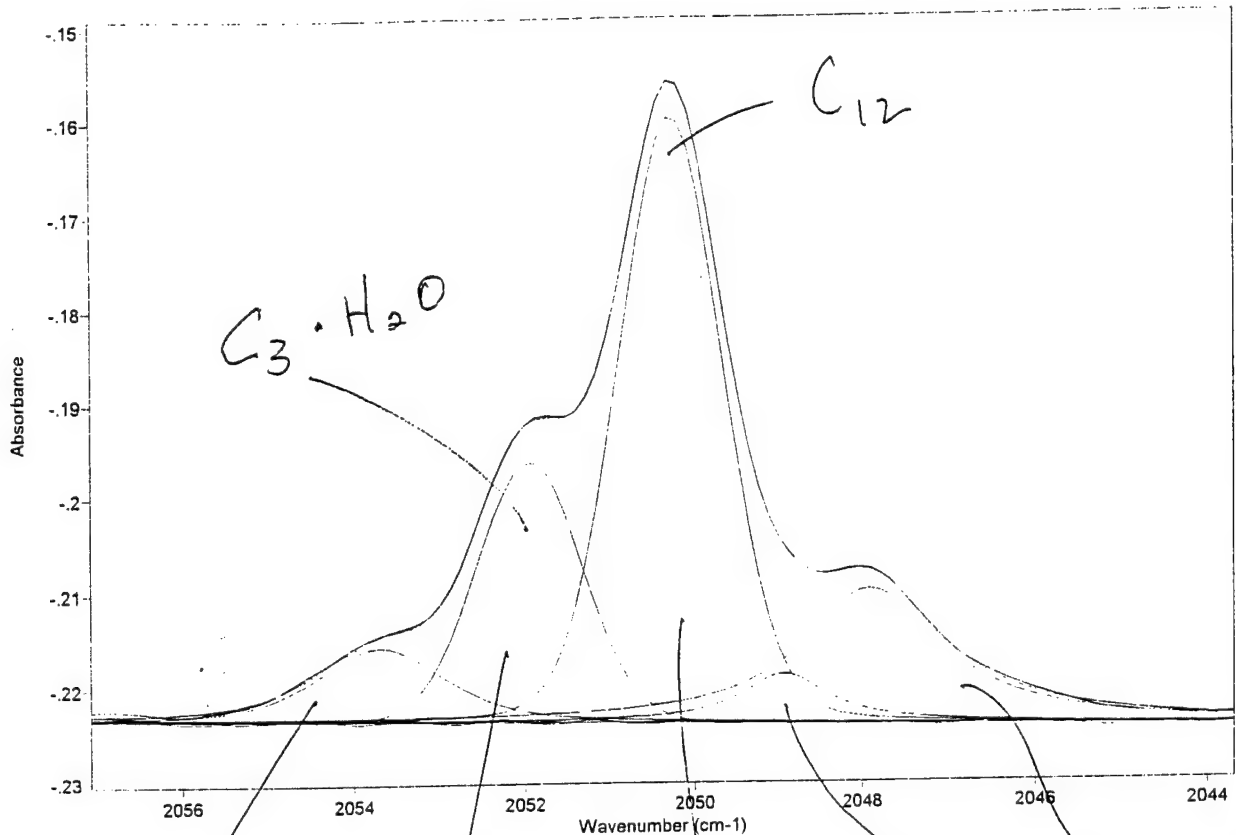
Cgrap501.spc
Curve Fit
Peaks
Residual

$N =$

| Peak# → | 1 | 2 | 3 | | 5 |
| width → | 1.7 | 1.4 | 1.4 | | 1.9 |

2053.7   2051.9   2050.3   2047.9
                                        2048.9

%lorentzian → 44%   0%   10%   4   99%
                                                1.2
                                                99%

Hanna Reslen —
cat of w/Wittig   (3f)

jL

Matrix C23

Cyclic C$_8$ Cyclic C$_6$

a(24)-a(23)
a(25)-a(24)
a(26)-a(25)
a(27)-a(26)
a(28)-a(27)
a(29)-a(28)
a(31)-a(29)
a(32)-a(31)

wavenumbers
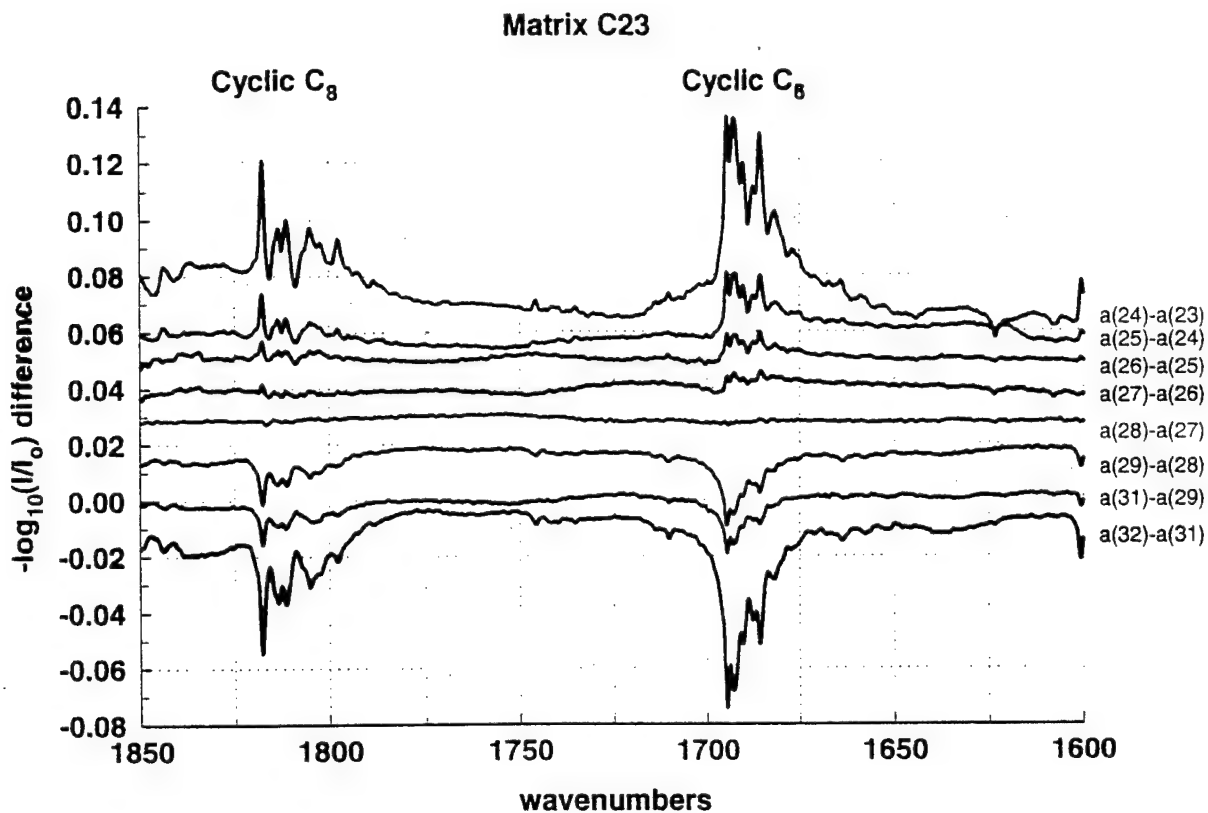
c6dif233.axg   Phillips Lab, Edwards AFB, CA 93524 Sept. 11, 1997 3:15:09 PM

Matrix C23 - 19% ^{13}C

CC6

C3

CC8

sC9

CC10 sC6 sC7
H2O C4 C5
sC11

annealing number

C23c2a.axg

15

C₃

n.

C③+ sink Arrhenius Plot

$k_{C3} = -t^{-1}\{((A_i - A_f)/A_{av})\}/s^{-1}$

M32
M39
M23
M49
M65

T^{-1}/K^{-1}
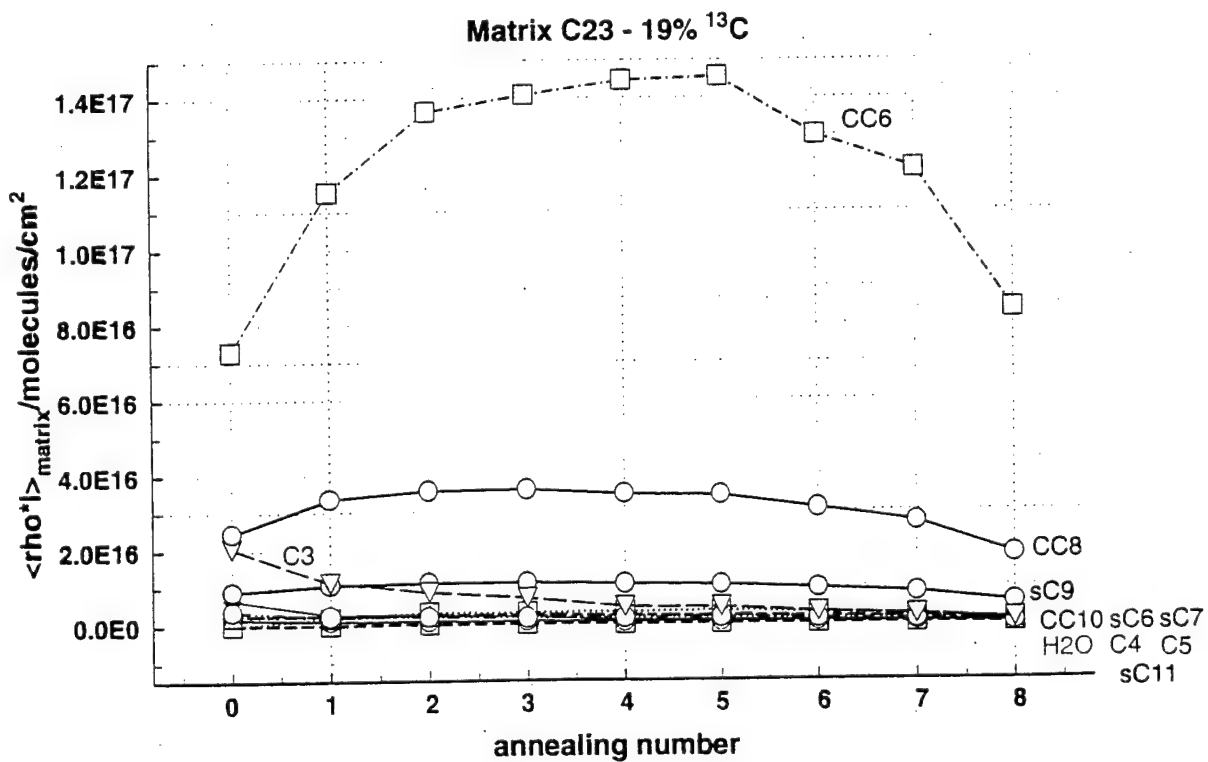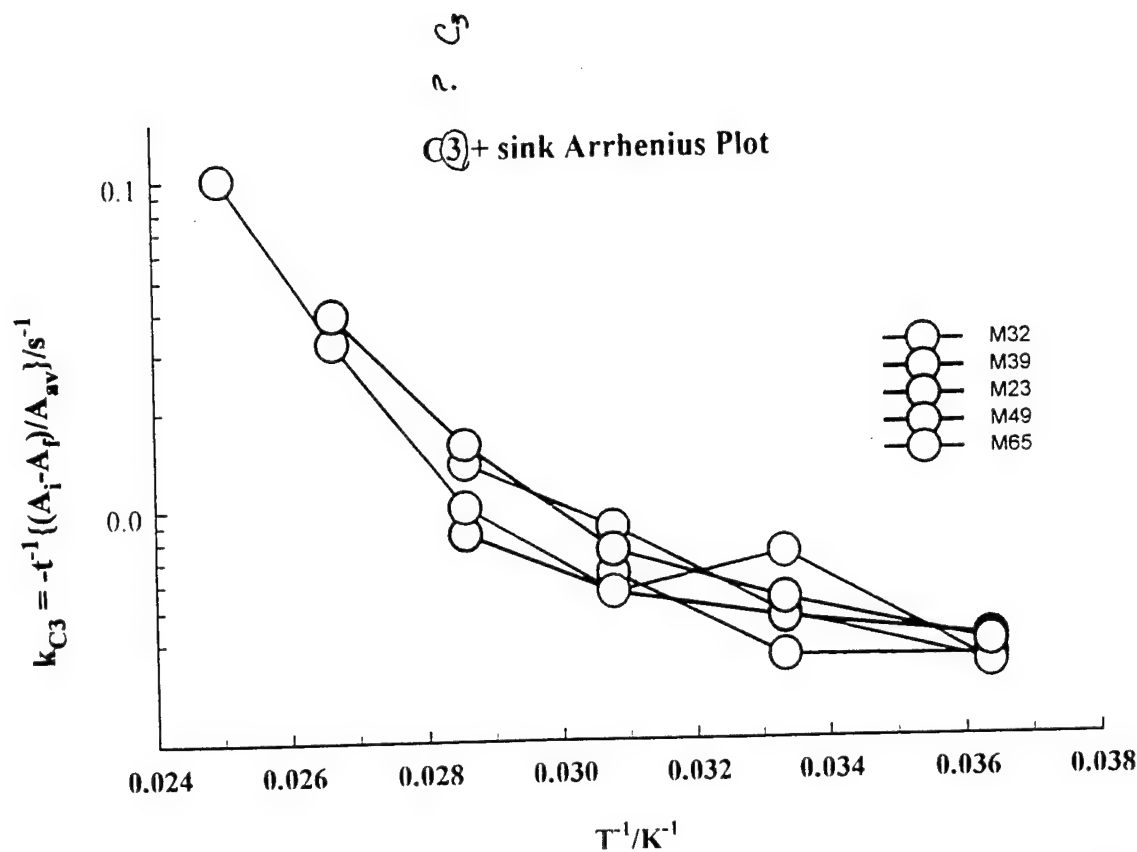
AM32c5.axg

Cyclic C_6 and Cyclic C_8 in High Carbon Density Hedm Prototypes,

Column Density $cC_6 + cC_8$/molecules/cm^2

C23

C75

C46

C52

B65

Ratio of Column Densities, cC_6/cC_8

MhiDsmy1.axg

$\nu_3 C_3$

2042 2037 2032

$\nu_3 C_4$

1548 1543 1538

$\nu_3 C_5$

2169 2164 2159

$\nu_4 C_6$

1957 1952 1947

$\nu_4 C_7$

2132 2127 2122

$\nu_5 C_8$

2076 2071 2066

$\nu_6 C_9$

2003 1998 1993

$\nu\ C_{10}$

2080 2075 2070
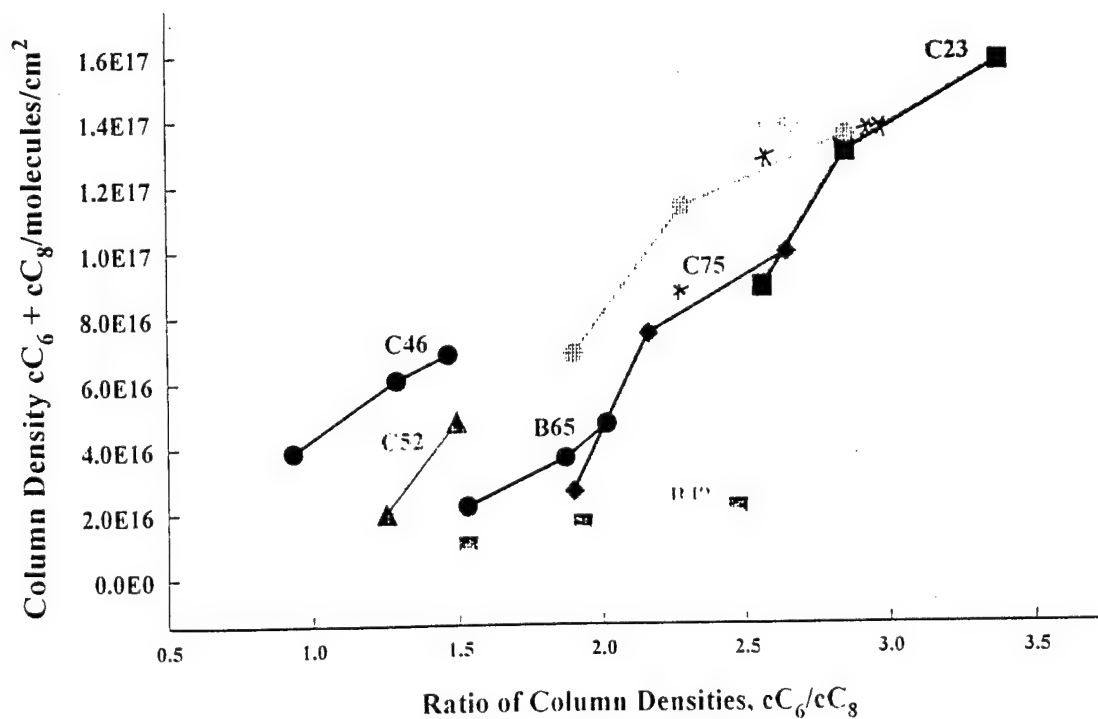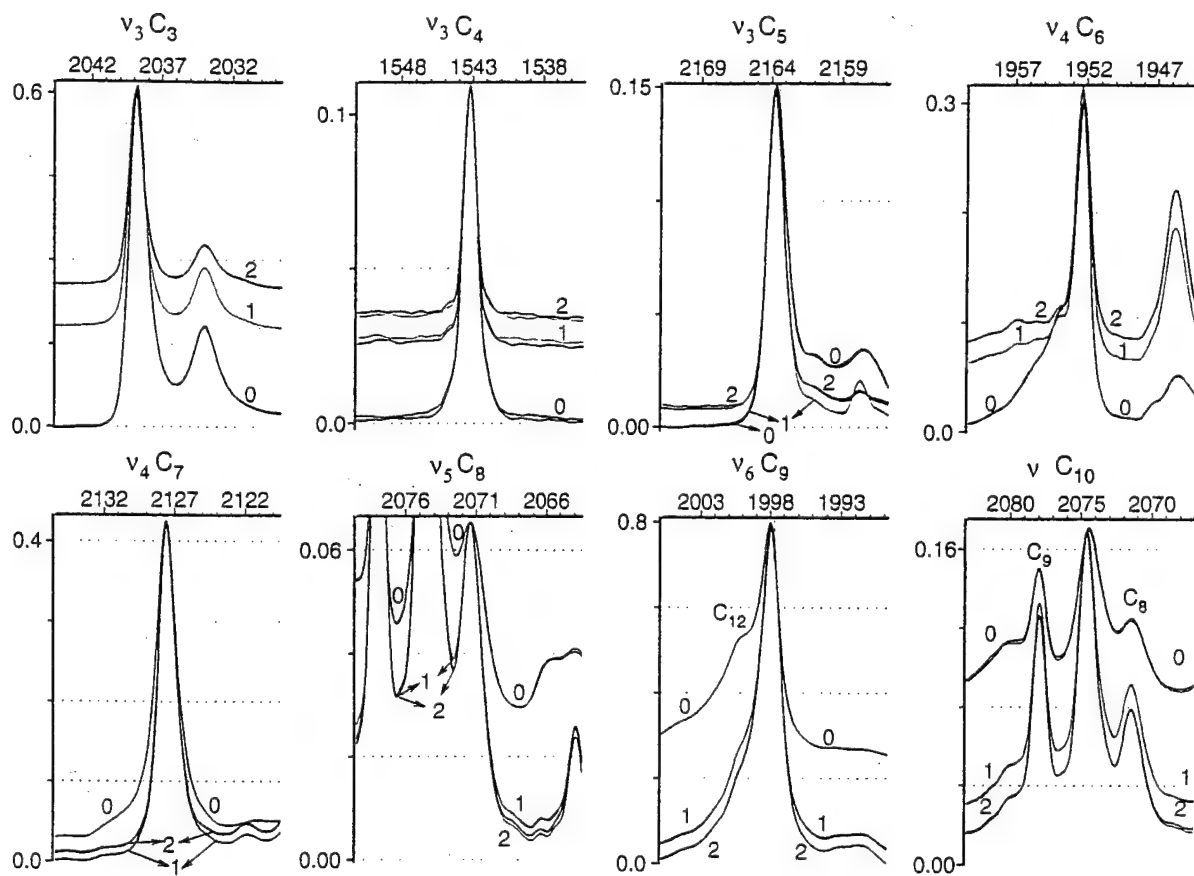
Carbon Matrix (a) - C_n Clusters

ν_4 cyclic C_6

1700 1695 1690

ν_{12} cyclic C_8

1822 1817 1812

CC10

1941 1936 1931

CC12

1951 1946 1941

TX 46

ν_4 cyclic C_6

1700 1695 1690

ν_{12} cyclic C_8

1822 1817 1812

CC10

1941 1936 1931

CC12

1951 1946 1941

JH03034

Carbon Matrix Tx 46 JA03034

17
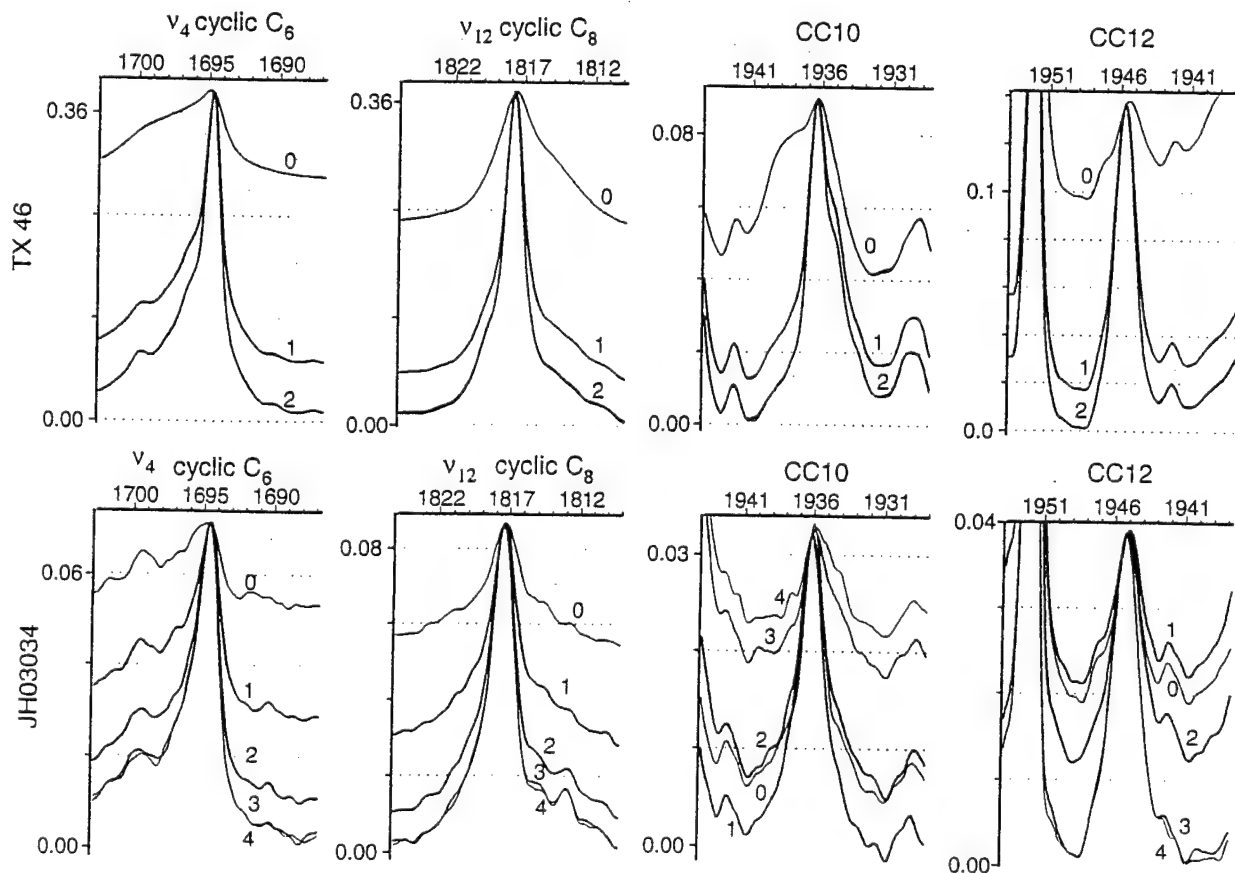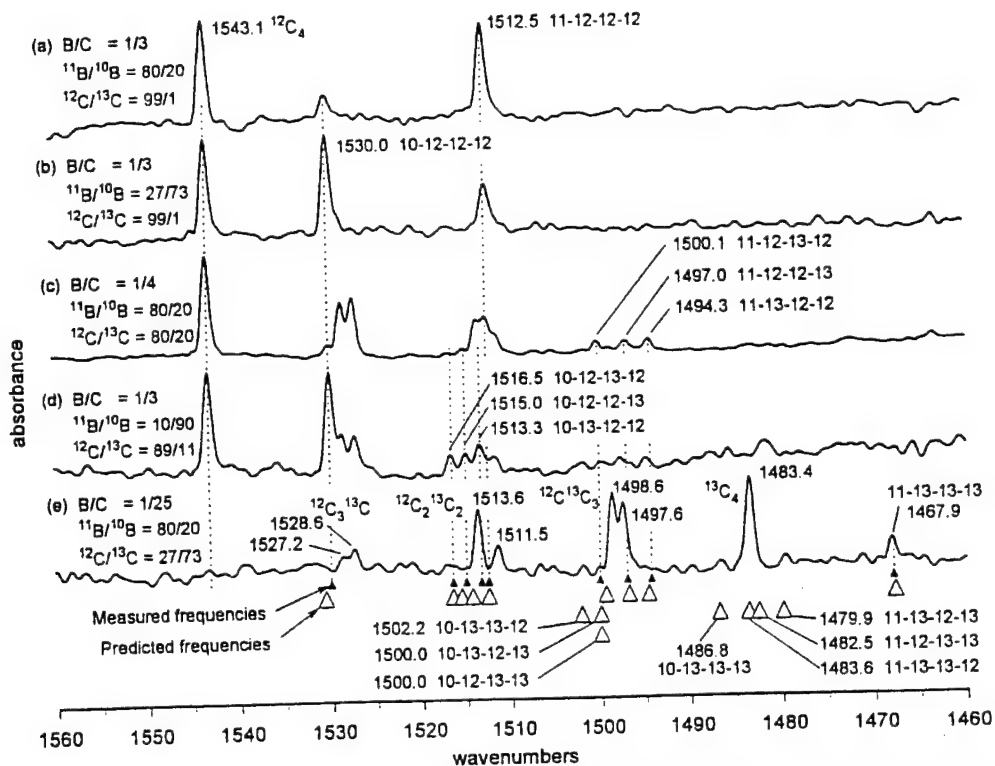
FIG. 1. FTIR spectra of the $\nu_2(\sigma)$ mode of isotopomers of linear BC_3 and the $\nu_3(\sigma_u)$ mode of isotopomers of linear C_4. The spectra were recorded at 10 K after annealing the matrices with the indicated compositions at 27.5 K for 150 s. The large open triangles at the bottom show the predicted frequencies of linear BC_3 isotopomers (as explained in the text) and small filled triangles show measured isotopomer frequencies.
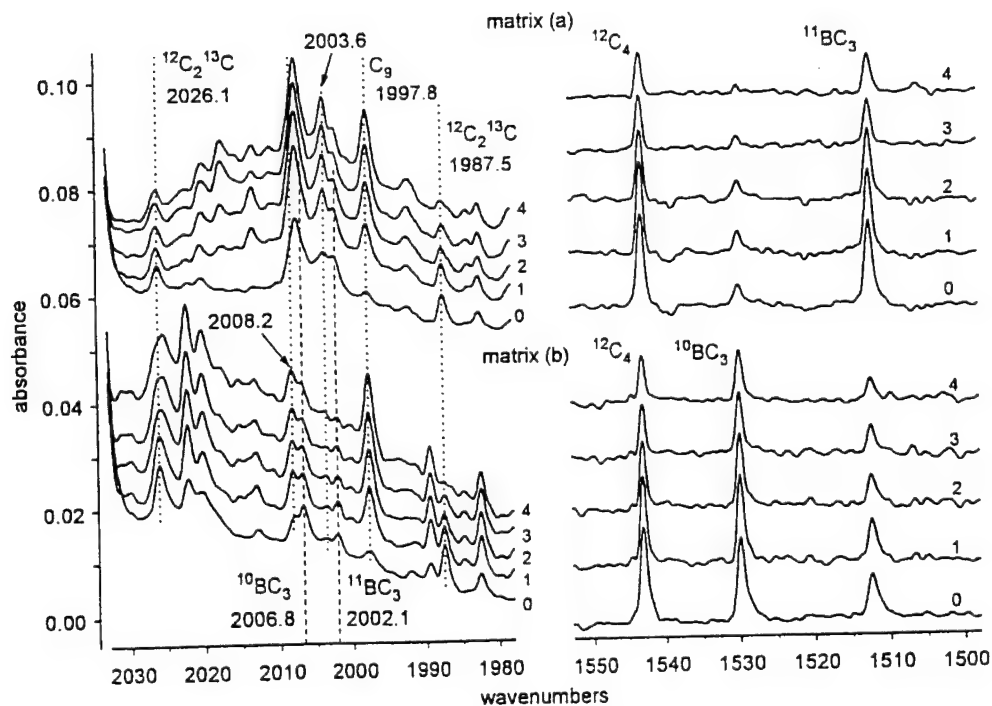
FIG. 2. Spectra obtained from matrix (a) [$^{11}B/^{10}B = 4/1$] and matrix (b) [$^{11}B/^{10}B = 1/2.7$] showing correlation upon annealing of the $\nu_1(\sigma)$ bands of $^{10}BC_3$ and $^{11}BC_3$ at 2006.8 and 2002.1 cm^{-1} with the $\nu_2(\sigma)$ bands at 1530.0 and 1512.5 cm^{-1}. The spectra labeled "0" are from the originally deposited matrix. Labels "1" to "4" indicate spectra recorded after the first through fourth annealing as follows: (1) 27.5 K for 150 s, (2) 30.0 K for 75 s, (3) 32.5 K for 45 s, (4) 35.0 K for 30 s. Frequency and absorbance scales are identical for all spectra. The plotted absorbance is $-\log_{10}$ of the transmittance. To facilitate comparisons between matrices, the absorbance of the matrix (b) spectra are multiplied by 1.4.
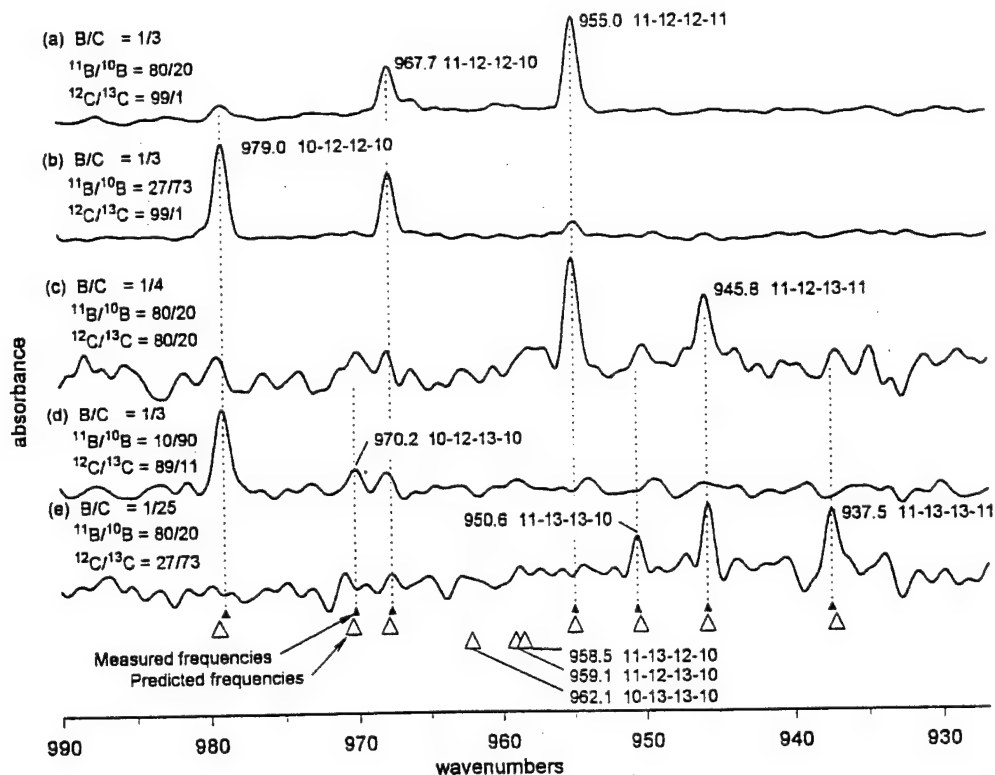
FIG. 3. FTIR spectra of the $\nu_3(\sigma_u)$ mode of isotopomers of linear BCCB. The spectra were recorded after annealing the matrices with the indicated compositions at 27.5 K for 150 s. The large open triangles at the bottom show the predicted frequencies of linear BCCB isotopomers (as explained in the text) and small filled triangles show measured isotopomer frequencies.

TABLE IV. Experimental B_2C_2 isotopomer frequency patterns. Frequencies and frequency intervals (cm^{-1}) in triplet bands of B_2C_2 isotopomers.

Boron isotope triplets				Carbon isotope triplets			
		Intervals				Intervals	
Isotopomer	Freq.	Short	Long	Isotopomer	Freq.	Short	Long
$^{10}B_2\,^{12}C_2$	979.0			$^{10}B_2\,^{12}C_2$	979.0		
		11.3				8.8	
$^{10,11}B_2\,^{12}C_2$	967.7		24.0	$^{10}B_2\,^{12,13}C_2$	970.2		$(16.7)^a$
		12.7				$(7.9)^a$	
$^{11}B_2\,^{12}C_2$	955.0			$^{10}B_2\,^{13}C_2$	$(962.3)^a$		
$^{10}B_2\,^{12,13}C_2$	970.2			$^{10,11}B_2\,^{12}C_2$	967.7		
		$(11.5)^a$				$(9.0)^a$	
$^{10,11}B_2\,^{12,13}C_2$	$(958.7)^a$		24.4	$^{10,11}B_2\,^{12,13}C_2$	$(958.7)^a$		17.1
		$(12.9)^a$				$(8.1)^a$	
$^{11}B_2\,^{12,13}C_2$	945.8			$^{10,11}B_2\,^{13}C_2$	950.6		
$^{10}B_2\,^{13}C_2$	$(962.3)^a$			$^{11}B_2\,^{12}C_2$	955.0		
		$(11.7)^a$				9.2	
$^{10,11}B_2\,^{13}C_2$	950.6		$(24.8)^a$	$^{11}B_2\,^{12,13}C_2$	945.8		17.5
		13.1				8.3	
$^{11}B_2\,^{13}C_2$	937.5			$^{11}B_2\,^{13}C_2$	937.5		

^{a}Frequencies and intervals in parentheses were interpolated or extrapolated from measured quantities.
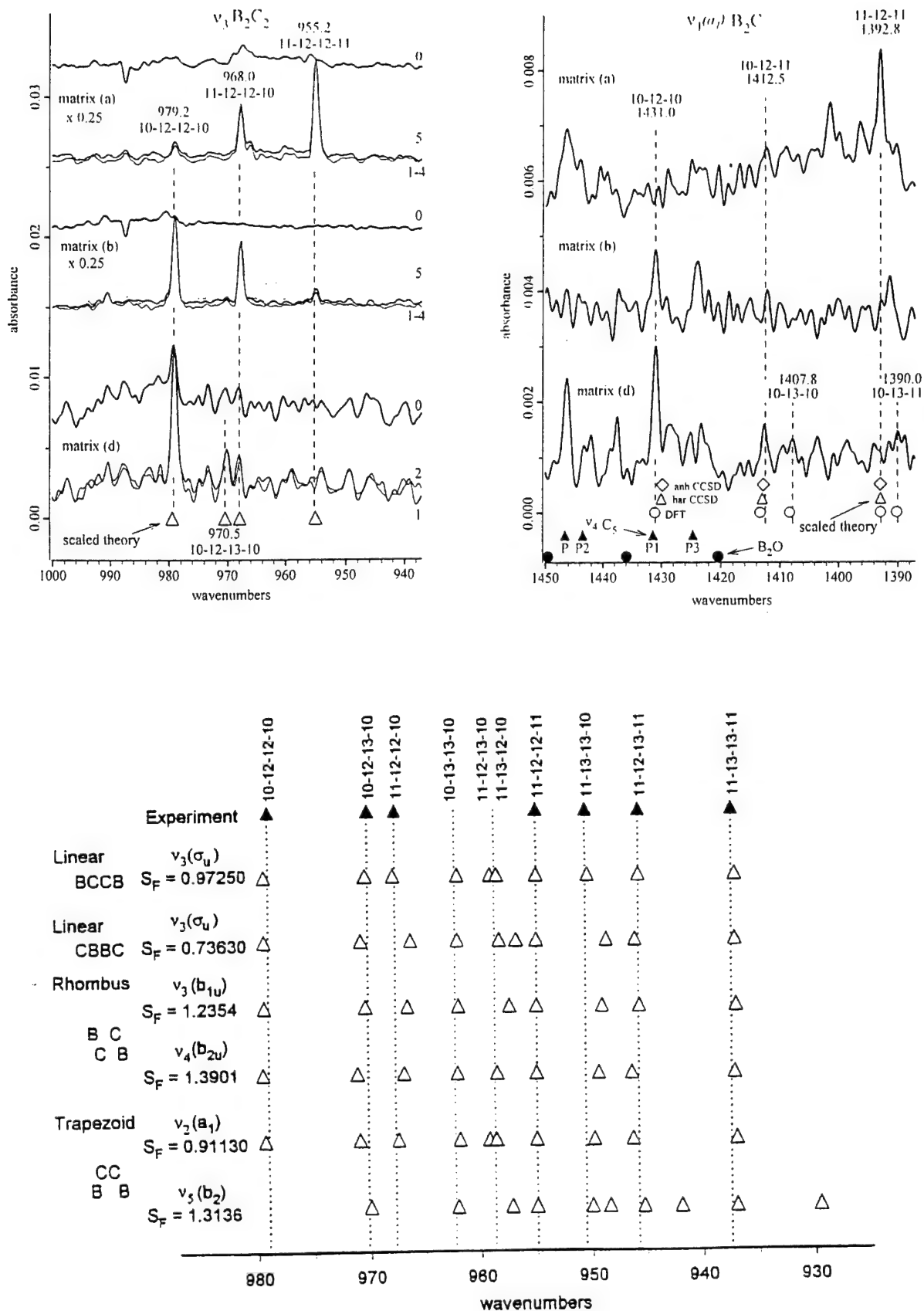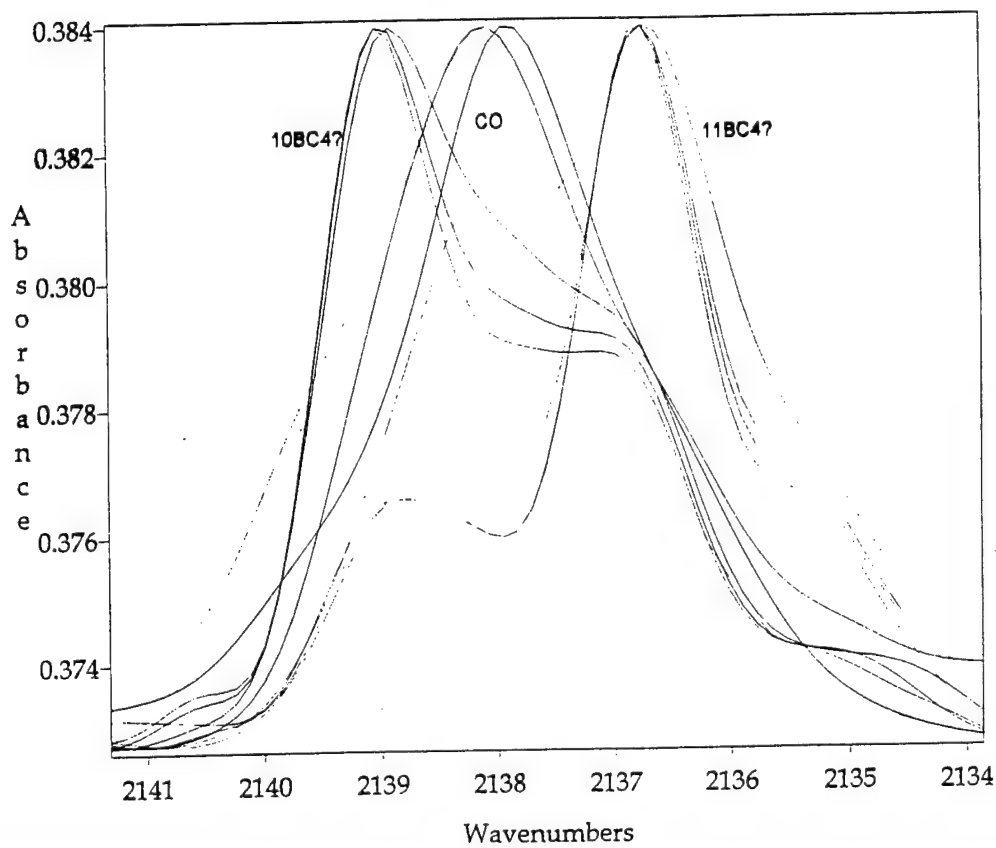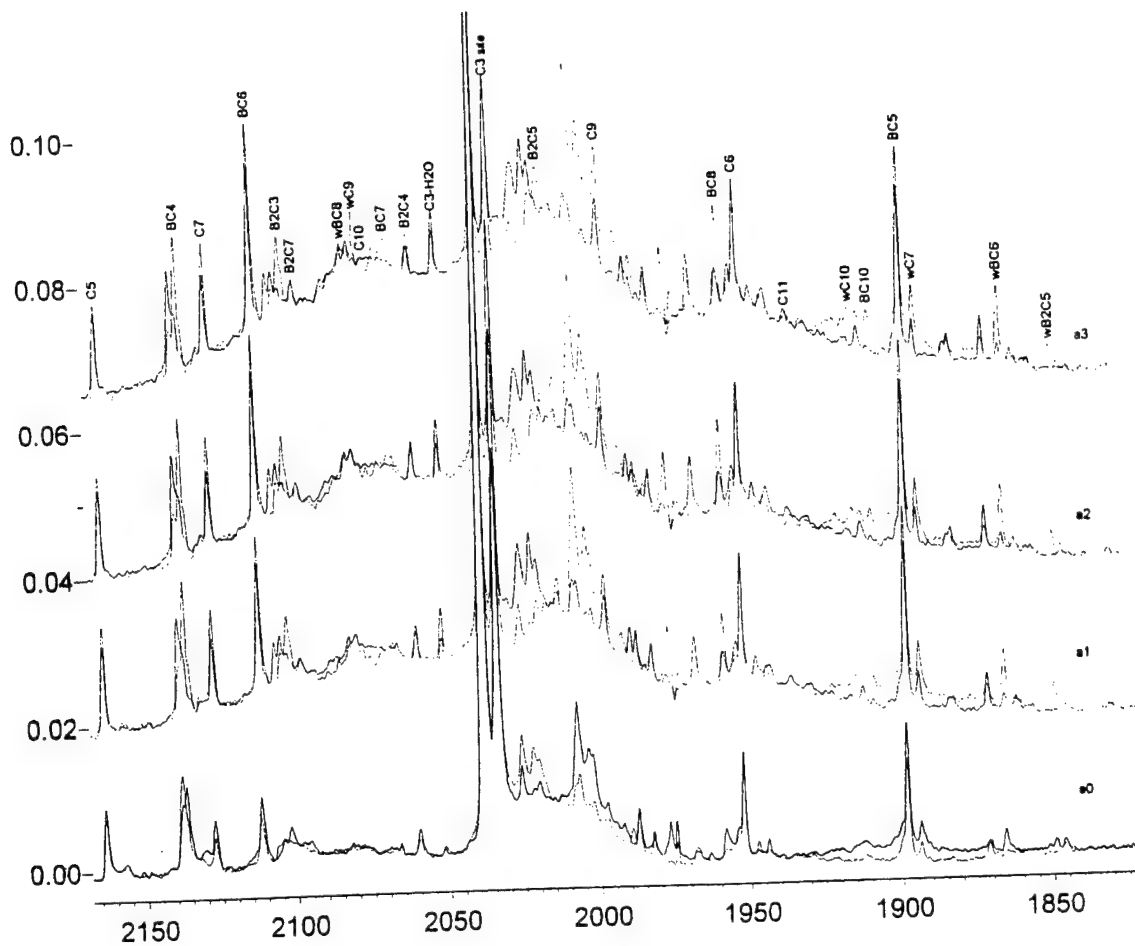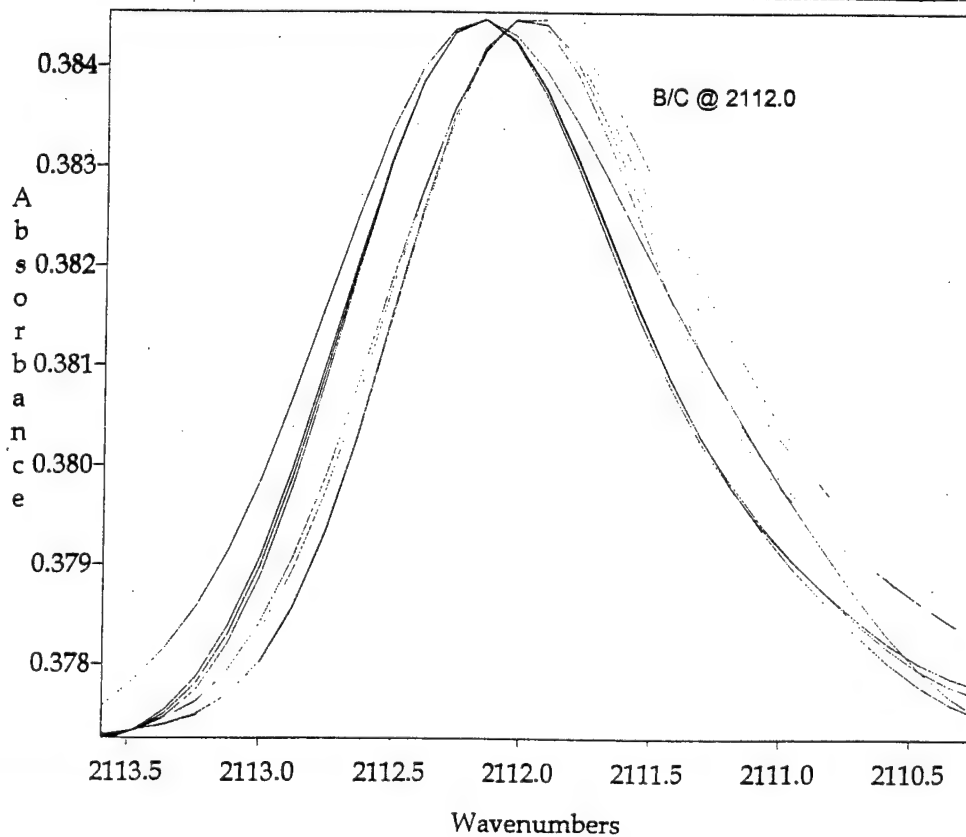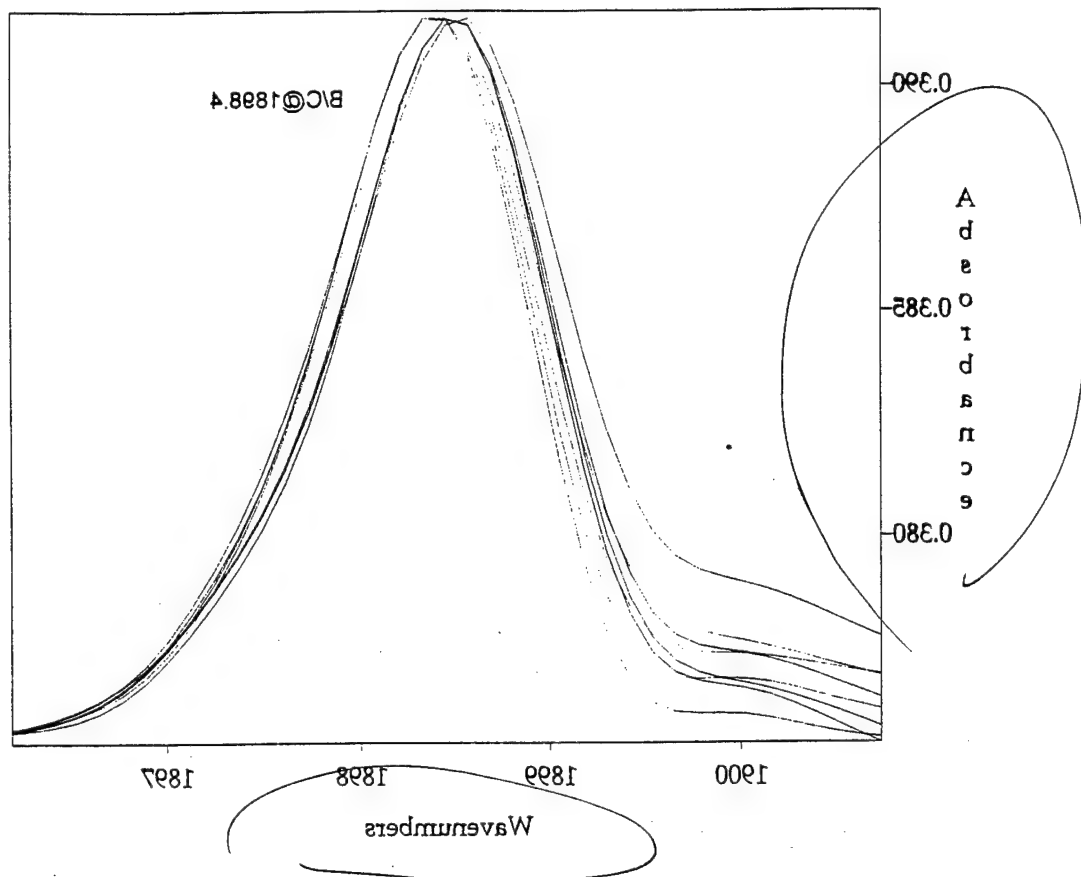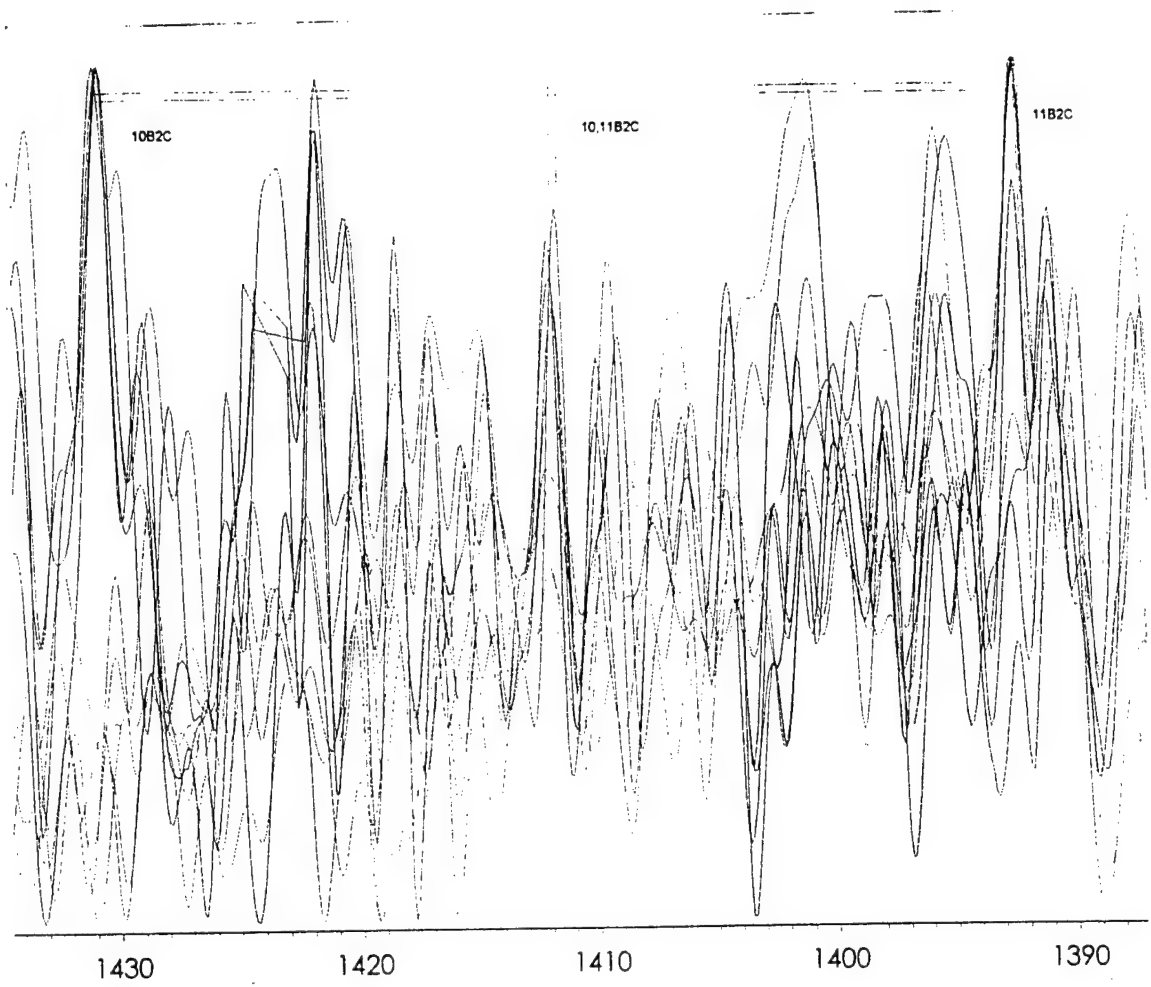
FIG. 4. Comparison of experimental isotopomer frequencies to scaled theoretical isotopomer frequencies for the most intense modes of four B_2C_2 geometries as calculated by Rittby, Ref. 5.
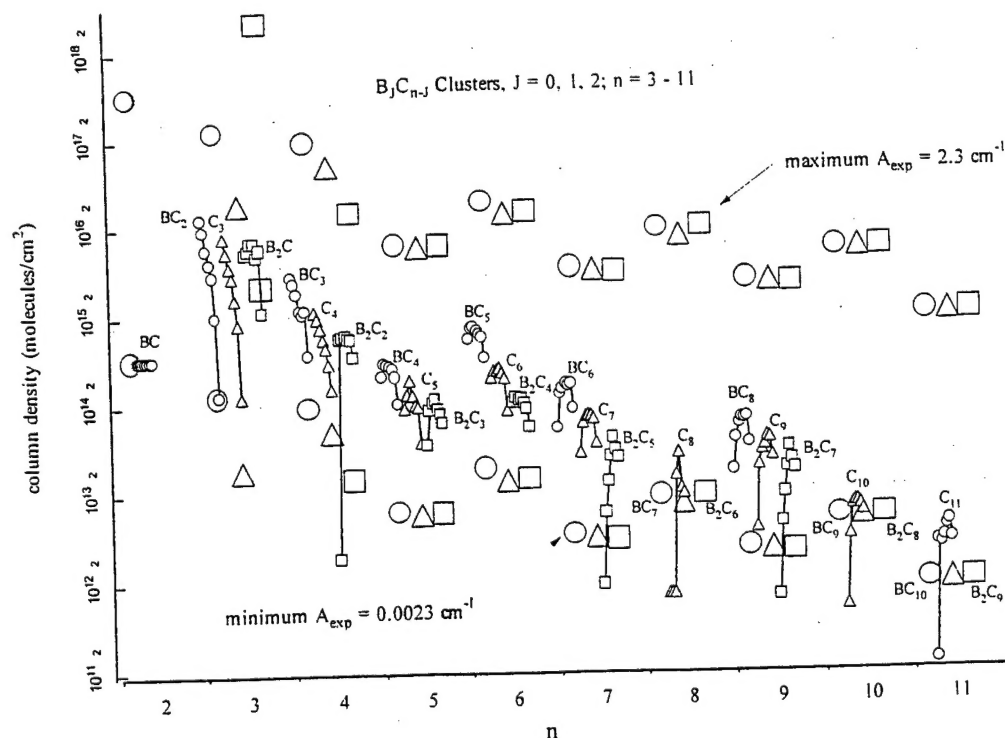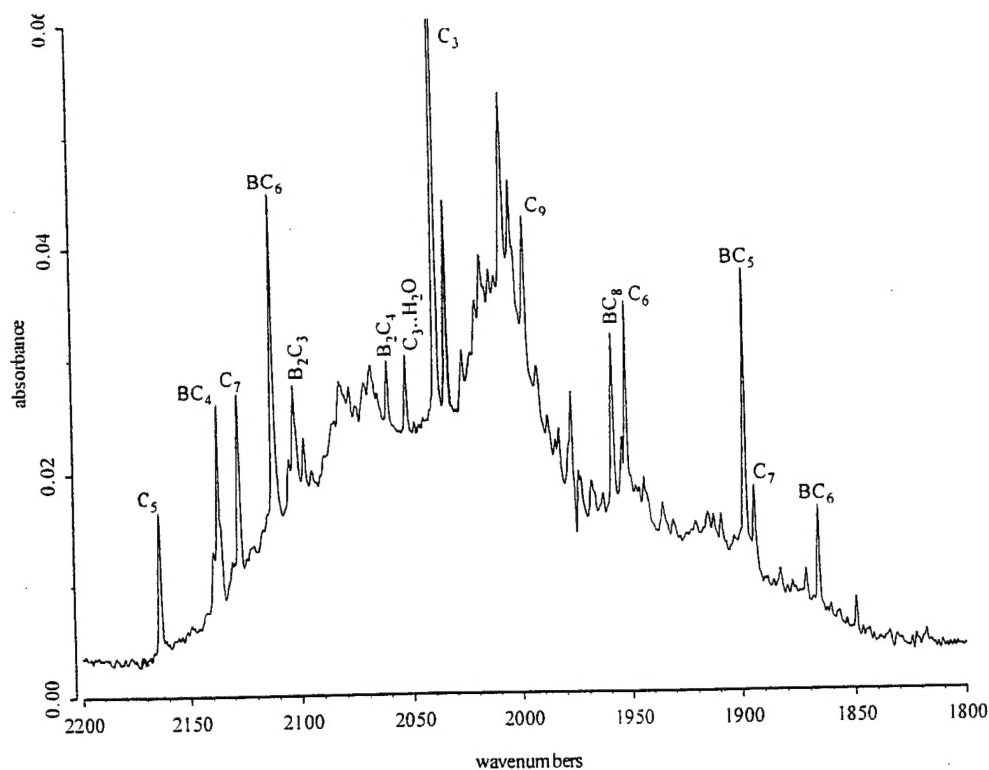
21

10B2C

10,11B2C

11B2C

1430   1420   1410   1400   1390

2L

Figure 1. Distribution of $B_J C_{n-J}$ clusters. $J = 0, 1, 2$; $n = 3 - 11$. Circles, triangles and squares represent BC_{n-1}, C_n, and BC_{n-2} clusters, respectively. Large symbols denote upper and lower limits of measurement, based on a nominal minimum measurable absorbance of 0.0023 cm^{-1}, and a maximum absorbance for linearity of Beer's law of 2.3 cm^{-1} (1% transmittance. Small symbols denote measured quantities in the initial matrix, and in six annealed matrices. Annealing temperatures and times were (1) 27.5 K/150 s, (2) 30.0 K/75 s, (3) 32.5 K/45 s, (4) 35.0 K/30 s, (5) 37.5 K/20 s, (6) 40.0 K/20 s. The decreases in column density in the fifth and sixth annealing are due to matrix sublimation. Some of the larger clusters ($n = 8, 10, 11$) have not been identified. BC_7, B_2C_6, BC_9, B_2C_8, BC_{10}, B_2C_9.
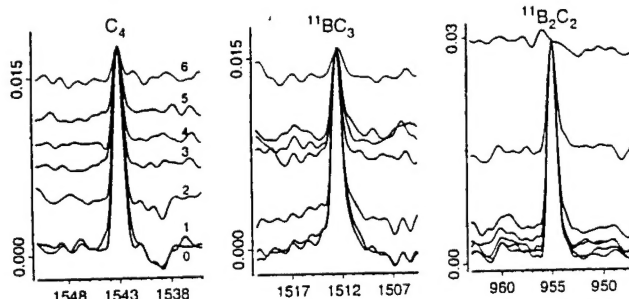
25

J = 0   1   2

matrix (a): $^{11}B/^{10}B = 80/20$, $^{12}C/^{13}C = 99/1$

n = 3

4
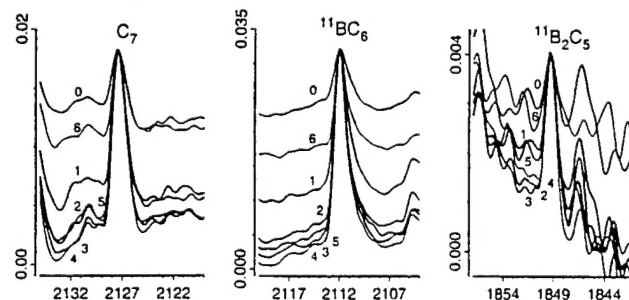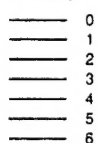
5

6
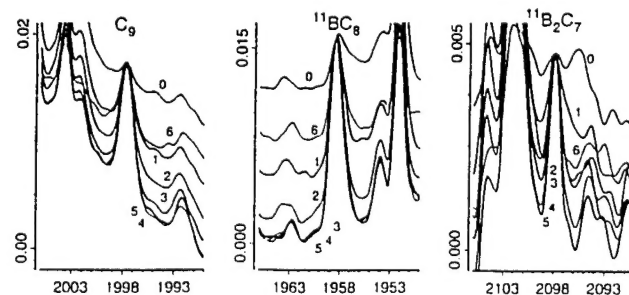
7
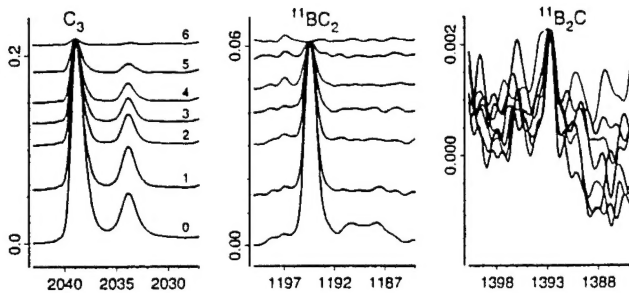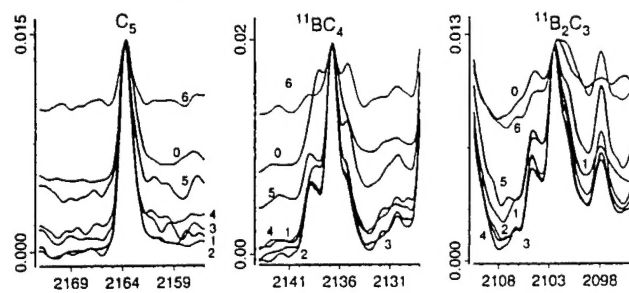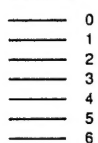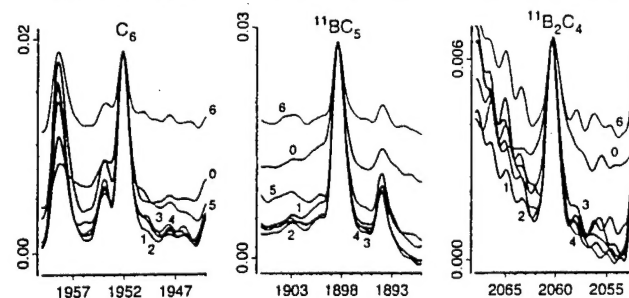
9

Conclusions

Linear C_3, cyclic BC_2, and cyclic B_2C, constituted about 80% of the total observable boron and carbon in the initially deposited matrix, but B_3 was not observed.

The measured trimer distribution in the initially formed matrices was
$$\rho(C_3) : \rho(BC_2) : \rho(B_2C) : \rho(B_3) \sim 1 : 1.5 : 0.5 : < 0.05.$$

Statistical substitution of J boron atoms into an n-atom carbon cluster produces a distribution given by $\rho(B_JC_{n-J}) / \rho(C_n) = [\{n(n-1)...(n-J+1)\}/J!] \, [B/C]^J$. With the experimental B/C $\sim$ 1/3, the statistical trimer distribution is
$$\rho(C_3) : \rho(BC_2) : \rho(B_2C) : \rho(B_3) \sim 1 : 1 : 0.33 : 0.03.$$

Agreement between distributions implies trimers form by random condensation of well-mixed atoms, uninfluenced by the relative energies of the trimers, the energies of their precursors, or preferential kinetics pathways that could otherwise distort the statistics.

Linear C_3 and cyclic BC_2, disappeared entirely when the matrices were repeatedly annealed to temperatures between 25 K and 35 K, but cyclic B_2C was inert.

Linear C_4 and BC_3 (BCCC) disappeared more slowly, and linear B_2C_2 (BCCB) grew to $\sim$ 95% of its final value during the first annealing. B_2C_2 was also inert, as B_2C.

The sources of B_2C_2 are from condensation of atom plus trimer ($B + BC_2$ but not $C + B_2C$) or dimer + dimer ($BC + BC$ but not $B_2 + C_2$). Although BC was not observed, the upper limit of $\rho(BC)$ is larger than $\rho(B_2C_2)$ so that BC cannot be ruled out as a source of B_2C_2.

The growth of B_2C_2 is conclusive evidence of the presence of BC and/or B in the originally deposited matrix in an amount at least as great as the growth of B_2C_2.

Linear C_5, BC_4 (BCCCC) and B_2C_3 (BCCCB)] and larger linear clusters (B_JC_{n-J}, $5 < n < 11$, $J = 0, 1, 2$), all grew upon annealing.

The sources of B_2C_3 are dimer + trimer ($BC + BC_2$ but not $B_2 + C_3$) and atom + tetramer ($B + BC_3$ but not $C + B_2C_2$).

Since $\rho(BC_2) \sim 5\rho(BC_3)$ in the initially deposited matrix, the $BC + BC_2$ source is dominant. Growth of B_2C_3 conclusively establishes the presence of BC in the matrix in an amount at least as great as the amount by which B_2C_3 grows.

Growth of BC_4 occurs primarily by $BC + C_3$ rather than $B + C_4$ or $C + BC_3$ because $\rho(C_3) \sim 10\rho(C_4)$ and $\rho(C_3) \sim 2\rho(BC_3)$. Growth of C_5 occurs by $C + C_4$ and $C_2 + C_3$, which establishes the presence of C and/or C_2 in the original matrix in an amount at least as great as C_5 growth.

Disappearance of triangular BC_2 requires breaking of one of its B-C bonds when one of its carbon atoms is attacked. The major reorganization of electronic energy involved in opening the ring appears to occur with little ($< \sim3$ kcal mol^{-1}) or no energy barrier, which makes this small molecule a candidate for an interesting *ab-initio* study of unusual reactivity at low temperature.

29

Conclusions

1. C_3 is linear but BC_2, B_2C and B_3 are cyclic.

2. $n > 3$; $J = 0, 1, 2$ clusters are linear. Boron atoms cap the ends of linear chains.

3. $J = 0, 1, 2$ substitution in $n \geq 5$ clusters does not significantly affect IR intensities.

4. For $n \geq 5$ the absorption intensity of even n clusters is two to three times smaller than that of odd n clusters.

5. B_2C_2 grew most dramatically upon annealing. BC was not detected. Its upper limit column density is comparable to that of $n = 4$ clusters. B_2C_2 sources may be 2BC or $B + BC_2$ but $C + B_2C$ does not form B_2C_2.

6. $n = 3, 4$; $J = 0, 1$ clusters disappear upon annealing but $J = 2$ clusters either grow or remain unchanged. Capping the ends of clusters with boron seems to render them inert to further condensation.

7. Statistical cluster distributions are apparent in $n = 4$ and 5 clusters. B_2C yields are too high and B_2C_{n-2} yields are too low in larger $n \geq 6$ clusters.

8. $n \geq 5$ clusters grow upon annealing and larger clusters grow more than smaller clusters.

Conclusions from Carbon HEDM Research

Quantitative analysis - Establishes HEDM density, distribution of carbon clusters, heat of formation of HEDM. Enables tracking of growth and decay of carbon clusters - carbon bookkeeping - quantification of "invisible carbon", C-atom and C_2.

Highest density matrix (equivalent C-atom density ~ 1 mole percent in argon) contained 40% "invisible" carbon (C, C_2), determined by tracking the growth of the "visible" (measurable) carbon to a constant composition after repeated annealing. Main product of condensation is cyclic C_6.

Yields of cyclic-C_6 are a factor of two larger than the combined yield of all other clusters in the fully condensed, highest density matrices. Cyclic-C_6 is the dominant condensation product.

Knudsen oven produces ~ 80% C_3 and ~ 10% each of C_2 and C-atom (by mass).
Laval oven with $\Delta T \sim 600$ K (between graphite surface and orifice) produces ~ 5% C_3 and C_2 and ~ 90% C-atom. C-atoms production by our oven (relative to C_3) is enhanced by higher temperature, which is accompanied by higher ΔT.

Substrate must be shielded from oven to prevent condensation during deposition.
Higher temperature oven places higher heat load on substrate, which promotes condensation.

Obtained higher density matrices by decreasing argon flux and maintaining oven flux. However, condensation was also increased.

One experiment with argon/5% H_2 caused nearly complete loss of C_{n+1} and C_{n+2} relative to C_{n+3}, suggesting that H_2 scavenges C-atoms efficiently during co-deposition.